Environmental Earth Sciences (2025) 84:434
https://doi.org/10.1007/s12665-025-12427-6

ORIGINAL ARTICLE

Biophysical parameters and land surface temperature dynamics in arid urban environments: A comprehensive machine learning approach

Hamad Ahmed Altuwaijri[1] · Abdulla Al Kafy[2] · Zullyadini A. Rahaman[3] · Jannatun Nahar Fariha[4] · Md Tanvir Miah[4] · Remon Ahmed Mishu[4] · Hrithik Nath[5,6] · M Shahriar Sonet[7,8]

Received: 18 December 2024 / Accepted: 5 July 2025 / Published online: 23 July 2025

Abstract

Urban heat islands (UHI) significantly affect urban sustainability, especially in arid cities facing rapid urbanization and climate change. This study aims to quantify the spatiotemporal variations in land surface temperature (LST) and identify key biophysical drivers affecting UHI patterns in Dammam, Saudi Arabia—an arid city experiencing rapid urbanization. We analyzed LST dynamics and their relationship with biophysical parameters over three decades (1993–2023) using Landsat imagery and advanced machine learning models, including Decision Tree (DT) and Random Forest (RF). Principal Component Analysis was employed to reduce data dimensionality and identify dominant thermal drivers. NDWI ($r = -0.652$), NDBI ($r = 0.590$), and NDVI ($r = -0.259$) emerged as the most significant predictors of LST, collectively explaining 78.6% of the thermal variance. The RF model significantly outperformed the DT model, explaining 88% of LST variance (95% CI: 0.862–0.906) with substantially lower mean squared error (0.151 vs. 0.274) and superior cross-validation performance across five folds (mean $R^2 = 0.884 \pm 0.025$). Results reveal significant thermal intensification over the study period, with mean LST rising from 29–32°C in 1993 to 44–47°C in 2023, indicating a warming rate of 0.485°C/year ($p < 0.001$). High-LST zones (> 44°C) expanded exponentially from 15 to 42% of Dammam's urban area, with built-up regions experiencing the most severe temperature increases (0.627°C/year). Water-related indices demonstrated the strongest cooling potential, with NDWI contributing 22.95% to model accuracy, followed by NDBI (19.06%) and NDVI (16.12%). Vegetation and moisture indices showed strong negative correlations with LST (NDVI: $r = -0.259$, 95% CI: -0.298 to -0.218; NDWI: $r = -0.652$, 95% CI: -0.689 to -0.612), while urbanization indices exhibited positive relationships. Bootstrap uncertainty analysis ($n = 1000$) showed prediction intervals of ± 2.1°C in vegetated areas to ± 3.4°C in heterogeneous zones. These findings emphasize the urgent need for climate-sensitive urban planning in arid environments, specifically recommending the integration of water features in high-NDBI zones (> 0.3) and mandatory 20% green space coverage in areas exceeding 44°C. This research provides a robust methodological framework for assessing thermal environments in similar arid regions and offers quantitative evidence for sustainable urban development strategies.

Keywords Land surface temperature · Urban heat island · Machine learning · Biophysical parameters · Remote sensing · Arid climate · Urban sustainability

Introduction

Rapid urbanization over the past few decades has fundamentally transformed land use and land cover patterns worldwide, resulting in elevated land surface temperature (LST) across metropolitan areas. The systematic replacement of natural vegetation with impervious surfaces creates the urban heat island (UHI) effect, a thermal phenomenon that poses significant ecological and socio-economic challenges, particularly affecting human health, energy consumption, and urban livability (Sonet et al. 2025; Choudhury et al. 2019; Das et al. 2021; Wu et al. 2016; Abdullah et al. 2022; Gogoi et al. 2019; Mukherjee & Singh 2020). This process not only contributes to biodiversity loss but also drives regional climate changes, making it essential to understand LST dynamics and their underlying drivers in order to develop effective mitigation strategies (Li et al. 2022; Liu et al. 2021a, b; Simkin et al. 2022; AlDousari et al., 2022).

Remote sensing (RS) and Geographic Information Systems (GIS) have emerged as powerful tools for investigating

Extended author information available on the last page of the article

LST patterns and quantifying UHI effects across diverse spatial and temporal scales. Contemporary research has revealed substantial spatial heterogeneity and seasonal variations in UHI intensity across different climatic regions, highlighting the complex nature of urban thermal environments (Ashwini et al. 2024; Faisal et al. 2021). These studies consistently demonstrate that urban surface materials, vegetation coverage, and water bodies play crucial roles in UHI mitigation, with this relationship being particularly pronounced in rapidly urbanizing Middle Eastern cities where extreme climate conditions amplify thermal stress (Gourfi et al. 2022; Han et al. 2023). Understanding these biophysical influences is fundamental for developing targeted urban climate adaptation strategies that address region-specific challenges (Salim et al. 2024; Yuan et al. 2022).

The relationship between land use/land cover (LULC) changes and LST fluctuations significantly impacts regional climate patterns and ecological systems (Das et al. 2020; Liu et al. 2021a, b). Researchers have extensively utilized RS-derived spectral indices to quantify these relationships, with the Normalized Difference Vegetation Index (NDVI) serving as a primary indicator of vegetation health and its cooling effect on urban temperatures (Weng et al. 2004; Hussain et al. 2022). Complementary indices, including the Normalized Difference Water Index (NDWI) and Modified Normalized Difference Water Index (MNDWI), have proven effective in assessing water body dynamics and their thermal influence. Additionally, the Normalized Difference Built-up Index (NDBI) and Soil-Adjusted Vegetation Index (SAVI) have been instrumental in examining urbanization-induced temperature variations across different landscape contexts (Hussain et al. 2023; Kafy et al. 2021; Sun et al. 2012).

Advanced machine learning (ML) approaches have revolutionized LST analysis, with techniques including Random Forest (RF), Artificial Neural Networks (ANN), and Support Vector Regression demonstrating superior performance in capturing complex thermal patterns (Ghosh & Joshi 2014; Malbéteau et al. 2017; Zhao et al. 2019). Traditional regression-based approaches often assume uniform parameter relationships across study areas, resulting in reduced accuracy when applied to spatially heterogeneous urban landscapes (Bisquert et al. 2016; Ghosh & Joshi 2014; Sattari et al. 2018; Weng et al. 2019a, b; Yang et al. 2017). This limitation necessitates the development of spatially explicit models capable of capturing localized variations in LST drivers and their interactions (Firozjaei et al. 2019).

Understanding spatial–temporal LST dynamics is essential for predicting future temperature trends and assessing their implications for urban sustainability and habitability. Land-use modeling techniques, exemplified by the Patch-generating Land Use Simulation (PLUS) model, provide valuable insights into LULC evolution and its cascading effects on urban thermal environments (Wang et al. 2022). Incorporating Principal Component Analysis (PCA) enhances the analytical framework by identifying dominant factors influencing LST variations across different temporal scales and enabling dimensionality reduction in complex datasets (Hall-Beyer 2003; Mirzaee & Mirzakhani Nafchi 2023). Given the accelerating urbanization in arid regions (Altuwaijri et al. 2025), developing comprehensive and location-specific analytical frameworks is crucial for improving LST prediction accuracy and designing effective mitigation strategies.

Despite substantial research progress in LST dynamics, critical knowledge gaps remain in understanding the complex interactions between biophysical indices and thermal patterns, particularly in rapidly urbanizing arid environments. While numerous studies have investigated these dynamics in temperate regions (Estoque et al. 2017; Guha & Govil 2022), considerably fewer have focused on arid regions where unique environmental conditions and urbanization patterns create distinct LST challenges. Cities in arid environments experience intense solar radiation, minimal precipitation, and heavy reliance on artificial cooling systems, which significantly amplify UHI effects compared to cities in more temperate climates (AlDousari et al., 2025). The coastal proximity and rapid industrialization of many arid cities introduce additional complexities in thermal regulation processes, creating specific microclimate conditions while industrial activities contribute to anthropogenic heat emissions that further intensify urban thermal stress.

The primary objective of this study is to analyze the relationship between LST and various biophysical indices in an arid urban environment, providing quantitative insights into urban thermal dynamics under extreme climatic conditions. This research examines how different biophysical factors influence LST patterns through the integration of RS techniques, advanced ML algorithms, and Principal Component Analysis (PCA). The methodological framework utilizes Google Earth Engine (GEE) and GIS to enhance predictive accuracy while accounting for non-linear relationships between biophysical parameters and thermal patterns. This approach enables comprehensive analysis of urban heat patterns and their underlying drivers.

By investigating the interactions between biophysical parameters and LST in a rapidly urbanizing arid region, this research contributes valuable knowledge to climate adaptation science and urban planning practices. The findings will provide evidence-based recommendations for policymakers designing sustainable urban development initiatives aimed at mitigating heat stress and improving environmental resilience under extreme climatic conditions. Additionally, this study establishes a methodological framework that can be applied to similar arid urban environments globally, supporting broader efforts to address urban heat challenges in the context of climate change and continued urbanization.

Materials and methods

Study area

Dammam City (26.32°N, 49.50°E) in Saudi Arabia's Eastern Province encompasses approximately 653 km^2 with 1,106,630 inhabitants, representing one of the most rapidly expanding urban centers in the Arabian Gulf region. The city exhibits diverse demographic characteristics, with Saudi nationals comprising 58% of the population while the remainder consists of international residents from Middle Eastern, Asian, and Western countries (Addas 2023; Rahman et al. 2017). Environmental characteristics are defined by a desert climate (Köppen BWh) featuring distinct seasonal patterns that significantly influence urban thermal dynamics. Summer months bring extreme heat exceeding 45 °C with high humidity due to coastal proximity to the Arabian Gulf. Winter conditions provide moderate relief (10–21 °C) with minimal precipitation throughout the year (Rahman et al. 2017). This climatic regime, combined with rapid urbanization and limited vegetation coverage, creates ideal conditions for investigating UHI effects and their relationship with biophysical parameters. The strategic coastal location introduces unique microclimatic conditions distinguishing it from inland arid cities, establishing it as an exemplary case study for understanding LST dynamics in rapidly urbanizing arid environments (Fig. 1).

Dataset description and selection criteria

The temporal analysis (1993–2023) was strategically designed to capture three decades of rapid urban transformation, coinciding with the region's most significant period of economic development and urban expansion (Rahman et al. 2017). This timeframe enables comprehensive analysis of LST dynamics across different urbanization phases

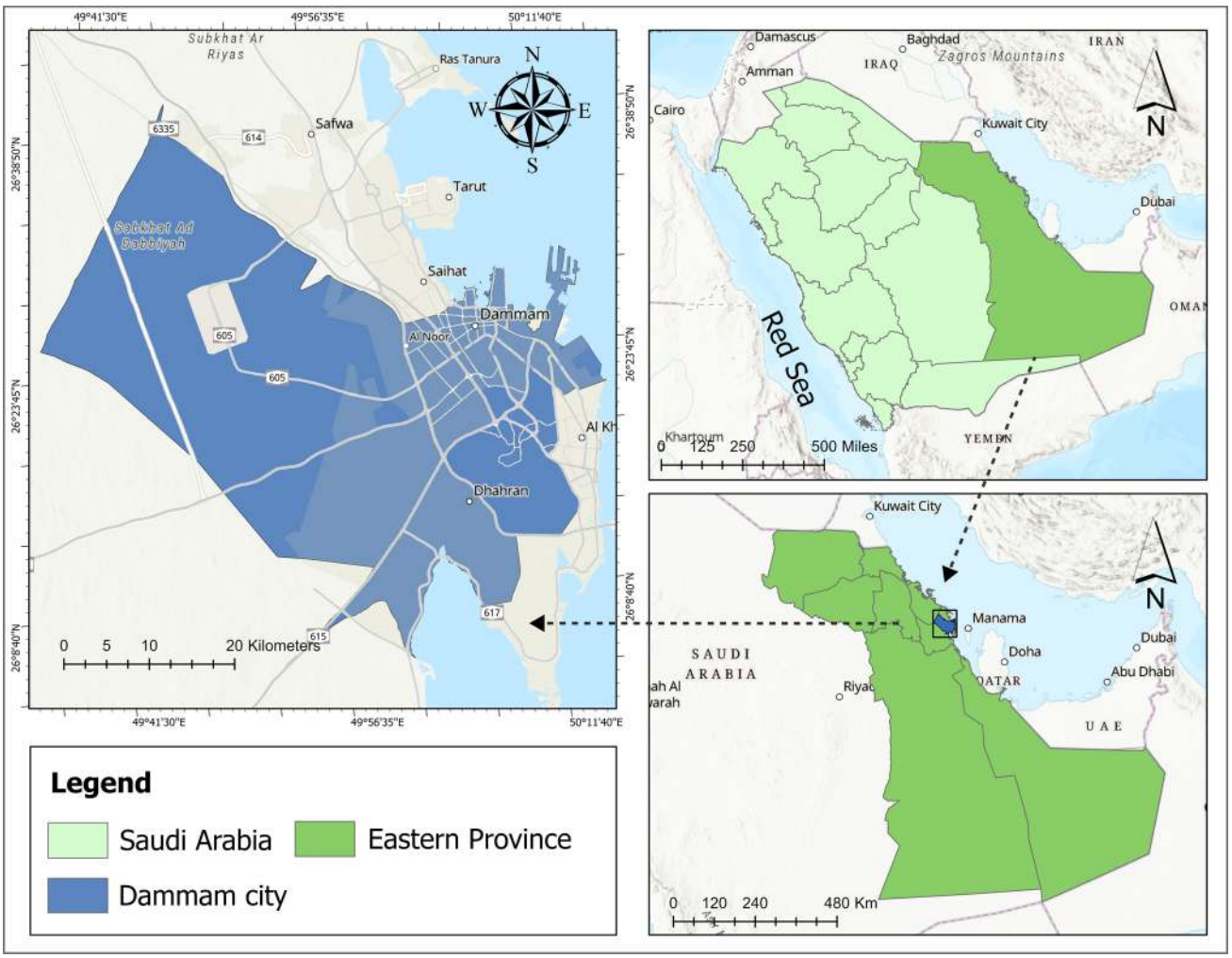

Fig. 1 Study area

while providing sufficient temporal resolution to identify long-term trends.

Landsat satellite imagery served as the primary data source due to its consistent temporal coverage, appropriate spatial resolution for urban-scale analysis, and availability of thermal infrared bands essential for LST retrieval. The multi-mission approach utilized Landsat 5 TM (1993–2011), Landsat 7 ETM + (1999–2013), and Landsat 8 OLI/TIRS (2013–2023), providing continuous coverage while maintaining data quality and cross-sensor compatibility.

Image selection was restricted to summer months (June–August) to minimize seasonal variations and capture peak thermal conditions when UHI effects are most pronounced in arid environments. The dataset was constrained to Landsat path/row 168/34, with all imagery accessed through USGS Earth Explorer (https://earthexplorer.usgs.gov). Conservative cloud cover threshold (< 10%) ensured data quality. This rigorous selection process identified 111 suitable images: 41 from Landsat 5, 38 from Landsat 7, and 32 from Landsat 8. Complementary meteorological data were obtained from regional climate observatories operating continuously from 1993 to 2023, providing ground-based measurements of air temperature, soil temperature, humidity levels, and surface temperature at various depths. Additional validation data were acquired from Terra satellite's MODIS sensor at 1000 m spatial resolution, accessed through NASA LAADS DAAC (https://ladsweb.nascom.nasa.gov). Figure 2 presents our analytical framework integrating image preprocessing, LST retrieval, PCA, and ML model development.

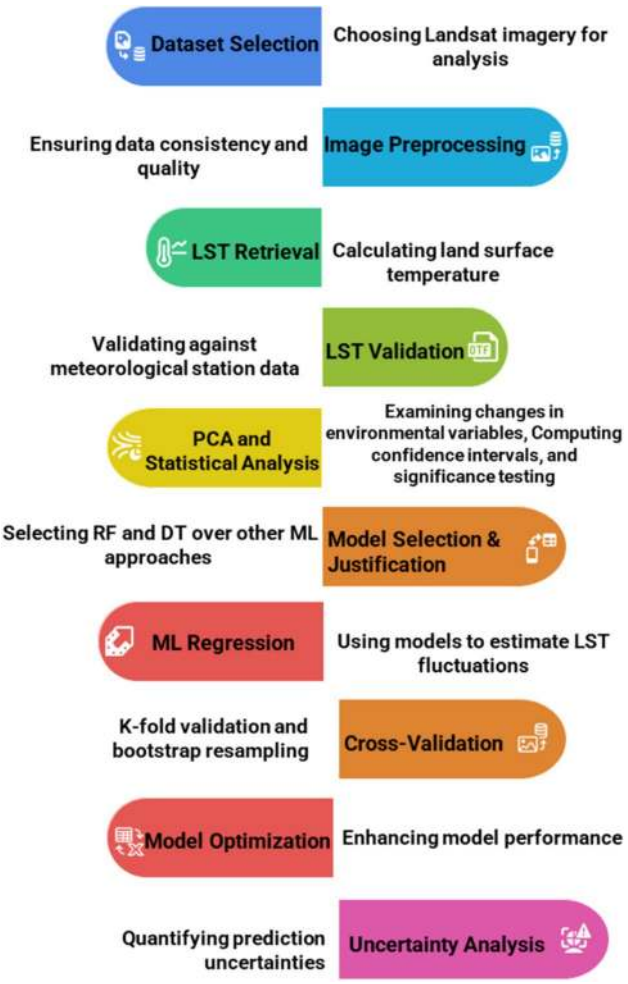

Fig. 2 Methodological framework

Image preprocessing and radiometric calibration

Comprehensive preprocessing procedures ensured data consistency and quality across the three Landsat sensor systems. Radiometric calibration followed standardized procedures (Chander et al. 2009; Mishra et al. 2014), converting digital numbers to top-of-atmosphere radiance using sensor-specific calibration coefficients. Surface reflectance values were derived through atmospheric correction utilizing the FLAASH algorithm, while inter-sensor calibration between different Landsat missions was conducted following standardized USGS procedures to ensure temporal consistency.

The Landsat 7 ETM + Scan Line Corrector (SLC) failure in May 2003 resulted in approximately 22% reduction in pixel coverage per scene (El Fellah et al. 2017). To address this data gap, a Neighborhood Similar Pixel Interpolator (NSPI) method was implemented following Chen et al. (2011). This interpolation technique operates on the principle that neighboring pixels of identical land cover classes possess similar spectral characteristics and exhibit comparable patterns of spectral variation, demonstrating particular effectiveness in recovering missing pixel values within heterogeneous urban environments while maintaining spatial accuracy and spectral integrity (Chen et al. 2011). Cloud masking procedures were performed using the Fmask algorithm with 10% cloud cover threshold to maintain data reliability and minimize atmospheric contamination. This comprehensive preprocessing workflow-maintained consistency across multiple Landsat sensors while preserving data integrity throughout the 30-year study period.

LST Retrieval, accuracy assessment and validation

For this study, the Single-Channel (SC) algorithm was selected for LST retrieval due to its demonstrated robustness in arid environments and superior ability to account for atmospheric effects compared to alternative methods. The algorithm incorporates atmospheric water vapor content and surface emissivity as key parameters, providing more accurate LST estimates in regions with high solar radiation and limited atmospheric moisture like Dammam (Jimenez-Munoz et al. 2014; Yu et al. 2014). As a result of bias and

notable inaccuracy in Landsat 8's thermal band 11 (Barsi et al. 2014), the SC algorithm was only able to calculate LST using band 10 for our analysis.

$$LST = \gamma\left[\frac{1}{\varepsilon}(\psi 1 L\lambda + \psi 2) + \psi 3\right] + \delta \quad (1)$$

where ε represents land surface emissivity calculated using the NDVI threshold method. y and δ are parameters derived from Planck's function. Ψ1, Ψ2, and Ψ3 are atmospheric functions determined using MODTRAN radiative transfer code.L$\lambda$is the at-sensor spectral radiance.

Landsat 5 and 8 thermal bands were used in this study to determine LST in Kelvin, with a spatial resolution of 30 m. The spectral radiance at the sensor (Lλ) in Watts/(m^2 sr μm) and land surface emissivity (ε) were utilized alongside parameters γ and δ derived from the Planck function (Jimenez-Munoz et al. 2014; Yu et al. 2014). The constants for the meteorological variables were ψ1, ψ2, and ψ3. For Landsat 8, only thermal band 10 (10.60–11.19 μm) was used due to calibration uncertainties in band 11, as documented by the USGS. The atmospheric parameters were calculated using Eq. 2 ($\Psi 1 = 0.14714w^2 - 0.15583w + 1.1234$), Eq. 3 ($\Psi 2 = -1.1836w^2 + 0.37607w - 0.52894$) and Eq. 4 ($\Psi 3 = -0.04554w^2 + 1.8719w - 0.39071$), where w is the total atmospheric water vapor content (g/cm^2) obtained from MODIS atmospheric profile product MOD07.. Land surface emissivity (LSE) was calculated using the NDVI threshold technique (NDVITHM). The effects of NDVI, SAVI, NDWI, NDBI, albedo, and TCT components (greenness, brightness, and wetness) on variations in LST were examined in Landsat 5, 7, and 8 images (Jiménez-Muñoz and Sobrino 2003; Sobrino et al. 2008).

Comprehensive validation procedures were implemented to assess the accuracy of satellite-derived LST estimates against ground-based temperature measurements. Ground truth data were obtained from the regional meteorological observatory, including air temperature measurements at 1.5m height and surface temperature measurements from 5 cm to 1 m above the surface. Validation was performed using contemporaneous measurements within ± 2 h of satellite overpass times to minimize temporal discrepancies. The validation methodology employed correlation analysis, Root Mean Square Error (RMSE) and Mean Absolute Error (MAE) calculations to quantify agreement between satellite-derived and ground-based measurements (Weng et al. 2019a, b; Yang et al. 2017). These validation metrics provide confidence in the reliability of LST retrieval methodology for subsequent analysis.

Biophysical parameter calculation

Seven biophysical indices were calculated from Landsat imagery based on their effectiveness in characterizing urban thermal environments and relevance to arid climate conditions (Table 1). NDVI served as the primary vegetation indicator due to its established LST relationship and reliability in arid environments (Weng et al. 2004; Hussain et al. 2022). SAVI was incorporated to address NDVI limitations in sparse vegetation areas through soil brightness correction (L = 0.5), providing accurate assessments in mixed urban-vegetation pixels (Ren et al. 2018).

NDWI was selected for detecting water bodies and assessing surface moisture content, factors significantly influencing LST in arid environments (Rad et al. 2021). Water indices show stronger LST correlations in arid regions compared to temperate climates (Guha et al. 2020a, b). Tasseled Cap Wetness provided independent moisture assessment, separating moisture-related spectral variation from other surface properties and offering insights into soil moisture patterns affecting urban thermal dynamics (Tabassum et al. 2024).

NDBI quantified urbanization intensity by identifying impervious surfaces through spectral characteristics of built-up materials (Arekhi et al. 2019). Tasseled Cap Brightness represented overall surface reflectance associated with

Table 1 Formulas for biophysical indices

Indices name and equations	References
$\mathbf{NDVI} = \frac{\rho NIR - \rho RED}{\rho NIR + \rho RED}$	(Abutaleb et al. 2015; Kumar et al.2022)
$\mathbf{NDWI} = \frac{\rho GREEN - \rho NIR}{\rho GREEN + \rho NIR}$	(Rad et al.2021)
$\mathbf{NDBI} = \frac{\rho SWIR - \rho NIR}{\rho SWIR + \rho NIR}$	(Arekhi et al. 2019)
$\mathbf{SAVI} = \left(\frac{\rho NIR - \rho RED}{\rho NIR + \rho RED + L}\right) * (1 + \boldsymbol{L})$	(Ren et al.2018)
Brightness = 0.303B + 0.279G + 0.473R + 0.560NIR + 0.508SWIR1 + 0.187SWIR2 (Landsat 8)	(Tabassum et al.2024 ; Surasinghe et al. 2025; Irulappa-Pillai-Vijayakumar et al. 2019)
Greenness = −0.2941B—0.243G—0.5424R + 0.7276NIR + 0.0713SWIR1—0.1608SWIR2 (Landsat 8)	
Wetness = 0.1511B + 0.1973G + 0.3283R + 0.3407NIR − 0.7117SWIR1 − 0.4559SWIR2	

impervious coverage and building materials (Surasinghe et al., 2025). Tasseled Cap Greenness provided alternative vegetation assessment capturing plant vigor aspects beyond NDVI and SAVI, particularly sensitive to chlorophyll content and plant structure (Bellón et al., 2017).

Recent advances in spectral index applications provide methodological insights for optimizing index combinations and implementing advanced regression techniques complementing ensemble learning methods (Liu et al. 2022; Al-Shaibah et al. 2021). All indices used sensor-specific coefficients ensuring temporal consistency across the 30-year study period. Tasseled Cap coefficients were adjusted for each Landsat sensor following established procedures to maintain spectral consistency (Tabassum et al. 2024).

PCA and temporal variation assessment

PCA was employed to examine temporal variations in environmental variables on a pixel-by-pixel basis following established methodologies (Dalal et al. 2010; Gaitani et al. 2017; Mas 1999; Weng et al. 2011). For each biophysical parameter and LST, PCA models temporal variations using n images within fixed intervals to identify dominant patterns of change. PC1 values provide insights into temporal stability: higher positive values indicate consistent pixel value increases over time, lower negative values suggest stable decreasing trends, while values near zero indicate significant temporal variability.

Normalization procedures were applied to mitigate climate-related differences and ensure comparable analysis across the 30-year study period. All parameters were rescaled to a uniform range of 0 to 1 using minimum and maximum values following Eq. 5:

$$\mathrm{NParameter}_i = \frac{\mathrm{Parameter}_i - \mathrm{Parameter}_{min}}{\mathrm{Parameter}_{max} + \mathrm{Parameter}_{min}} \quad (2)$$

ML implementation

DT and RF models analyzed LST-biophysical relationships using PC1 values. Implementation included: (a) feature normalization; (b) 70% training/30% testing split with stratified sampling; (c) hyperparameter optimization via grid search with fivefold cross-validation; (d) performance evaluation using R^2, MSE, RMSE, MAE. DT optimization employed tree depth calibration via cross-validation to balance model complexity and accuracy, addressing overfitting in complex datasets (Xu et al. 2005). Splitting criteria used minimum sample split of 10 with cost-complexity pruning to mitigate overfitting risks (Breiman et al. 2017; Quinlan 1993). RF parameters were calibrated through grid search optimization determining maximum depth (Rodriguez-Galiano et al. 2012). Feature selection based on Gini importance scores retained variables exceeding 0.05 threshold, aligning with established RS practices for spatially heterogeneous landscapes (Bisquert et al. 2016; Yang et al. 2017).

Validation protocols allocated 70% for training and 30% for testing with stratified sampling ensuring representative temperature distributions across diverse thermal zones (Shafizadeh-Moghadam et al. 2020). Five-fold stratified cross-validation provided robust evaluation accounting for temporal autocorrelation in the 30-year dataset (Hall-Beyer 2003). Performance evaluation employed MSE, R^2, p-values, and standard error metrics (Hutcheson & Hutcheson 2011). DT regression minimizes variance through systematic data segmentation (Breiman et al. 2017; Quinlan 1993; Xu et al. 2005). RF ensemble learning reduces overfitting while capturing non-linear relationships (Rodriguez-Galiano et al. 2012). Model optimization addressed overfitting through tree depth calibration, cost-complexity pruning, and Gini importance-based feature selection (>0.05 threshold) following established RS practices (Bisquert et al. 2016; Yang et al. 2017). Validation protocols ensured robust evaluation across thermal conditions using stratified cross-validation accounting for temporal autocorrelation (Hall-Beyer 2003; Shafizadeh-Moghadam et al. 2020). Performance metrics provided comprehensive accuracy assessment (Hutcheson & Hutcheson 2011).

Bootstrap resampling ($n=1000$) estimated 90% prediction intervals following environmental modeling practices (Crank et al. 2020). RF ensemble learning incorporated aleatory and epistemic uncertainties (Mathew et al. 2024). Spatial autocorrelation analysis using Moran's I assessed error patterns (Bisquert et al. 2016), while Monte Carlo simulation quantified parameter sensitivity. Quantile regression forests determined spatially varying prediction intervals across landscape types (Meinshausen 2006).

Results

Spatial and temporal distribution of LST

The temporal evolution of LST from 1993 to 2023 reveals dramatic thermal intensification patterns reflecting rapid urbanization. Figure 3 illustrates comprehensive LST maps spanning the 30-year study period, with images strategically selected from summer months (June–August) to minimize seasonal variations and ensure accurate temporal comparisons.

In 1993, baseline conditions showed moderate temperatures (29–32°C) with cooler zones below 26 °C in areas with sparse development and vegetation coverage. The spatial distribution indicated relatively uniform thermal conditions reflecting limited urban development during the early 1990s.

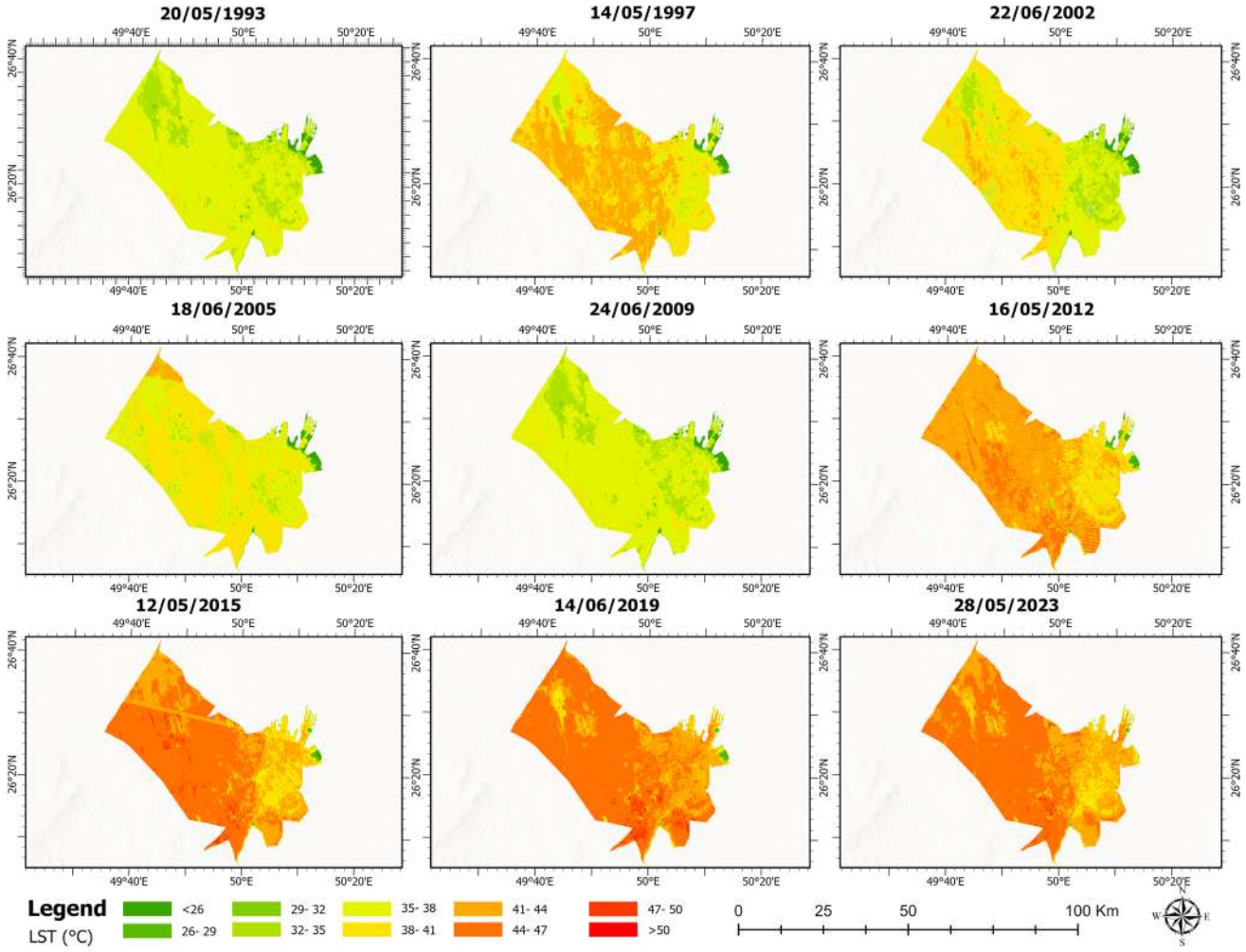

Fig. 3 LST maps (°C), illustrating the period of 1993–2023 in Dammam City, Saudi Arabia

By 1997, notable thermal intensification occurred with most areas experiencing elevated temperatures (41–44°C), indicating significant warming of approximately 12–15°C within four years.

The period from 2002–2005 showed continued thermal stress (38–41°C), suggesting some stabilization during the mid-2000s. However, year 2009 exhibited temporary cooling anomaly (32–35°C) likely associated with specific climatic conditions, followed by accelerated warming post-2009 with 2012 showing extensive areas at 41–44°C.

The most concerning trends emerged in the final decade. By 2015, 2019, and 2023, extensive portions consistently experienced extreme temperatures (44–47°C), with some regions exceeding 50°C. This represents critical escalation in urban thermal stress, with highest temperature zones expanding spatially to cover increasing proportions of the urban area, clearly demonstrating accelerating UHI intensification corresponding with rapid urban expansion.

Statistical analysis reveals statistically significant increase in mean LST ($\beta = 0.485$°C/year, $p < 0.001$, $R^2 = 0.823$), with most pronounced warming in built-up areas (0.627°C/year, 95% CI: 0.589–0.665°C/year). High-LST zones (> 44 °C) expanded exponentially from 15% to 42% of the urban area, representing nearly three-fold increase in extreme thermal stress zones. The spatial pattern shows clear correlation with urban development patterns, with most intense warming in areas of rapid infrastructure development and population density increases.

Statistical relationships between LST and biophysical parameters

Table 2 presents comprehensive statistical relationships between LST and surface biophysical parameters with 95% confidence intervals. All parameters demonstrate statistically significant relationships (P-values < 0.001), indicating

Table 2 Statistical relationships between LST and surface biophysical parameters with 95% confidence intervals

Surface BPs	*R* value	95% CI Lower	95% CI Upper	*P* value	Std. dev
Brightness	0.55**	0.506	0.591	< 0.001	0.098
Greenness	−0.259*	−0.298	−0.218	< 0.001	0.18
NDBI	0.59**	0.548	0.628	< 0.001	0.083
NDVI	−0.259*	−0.298	−0.218	< 0.001	0.093
NDWI	−0.652**	−0.689	−0.612	< 0.001	0.078
SAVI	−0.363**	−0.405	−0.319	< 0.001	0.062
Wetness	0.551**	0.507	0.592	< 0.001	0.095

**Correlation is significant at $p < 0.001$ level

*Negative correlation indicates cooling effect

robust associations between surface characteristics and thermal conditions.

Water-related indices exhibit the strongest negative correlations with LST, with NDWI showing the most potent cooling effect ($r = -0.652$, 95% CI: −0.689 to −0.612). This underscores the critical importance of water features and surface moisture in mitigating urban heat in arid environments. Vegetation indices demonstrate moderate but significant negative correlations: NDVI ($r = -0.259$, 95% CI: −0.298 to −0.218) and SAVI ($r = -0.363$, 95% CI: −0.405 to −0.319). The stronger SAVI correlation suggests soil-adjusted vegetation assessments provide more accurate representation of cooling effects where soil background interference affects traditional vegetation indices.

Tasseled Cap components reveal contrasting relationships reflecting different surface characteristics. Greenness shows negative correlation ($r = -0.259$, 95% CI: −0.298 to −0.218) consistent with vegetation cooling effects, while Wetness demonstrates the strongest negative relationship ($r = -0.652$, 95% CI: −0.689 to −0.612), emphasizing surface moisture importance in thermal regulation.

Urban development indicators show strong positive correlations confirming their role in UHI intensification. NDBI exhibits substantial positive correlation ($r = 0.590$, 95% CI: 0.548–0.628), indicating built-up areas consistently experience elevated temperatures. Brightness demonstrates similarly strong positive relationship ($r = 0.550$, 95% CI: 0.506–0.591), reflecting thermal impact of high-albedo urban materials that absorb and re-radiate heat effectively.

Low standard deviation values (approximately 0.1) across all parameters indicate tightly clustered data points, demonstrating consistent and reliable relationships. High-NDBI areas (> 0.4) consistently exhibit LST values > 46 °C, while areas with elevated NDWI values maintain 3–5 °C lower temperatures. The exceptional NDWI cooling effect ($r = -0.652$) exceeds similar studies in temperate zones (typically $r = -0.3$ to -0.5) due to amplified thermal contrast between water surfaces and surrounding arid landscape, where moisture scarcity makes any water presence thermally significant.

PCA and temporal variation patterns

Figure 4 presents PC1 patterns for LST and associated biophysical parameters, revealing distinct spatial clusters with unique thermal characteristics. The PC1 maps effectively capture dominant modes of temporal variation, providing insights into areas of thermal stability versus change over the 30-year study period.

Red regions consistently exhibit high pixel values across multiple temporal observations, suggesting minimal temporal variation and stable thermal conditions. These areas predominantly represent urbanized landscapes with high impervious surface coverage, evidenced by elevated PC1 values for LST, Brightness, and NDBI components. The spatial correspondence between high LST PC1 values and urban development indicators confirms that urbanization leads to consistent temperature elevation due to thermal properties of built-up materials.

Blue regions consistently display low PC1 values, indicating different but equally stable thermal conditions. These areas correspond to zones with lower baseline temperatures, reduced brightness, and limited urban development. Low PC1 values for NDVI, NDWI, and SAVI suggest sparse vegetation, limited water presence, or undeveloped land maintaining relatively stable thermal properties over time.

Areas with PC1 values approaching zero represent the most dynamic zones, suggesting significant land-use transitions during the study period. These pixels likely indicate areas experiencing substantial transformation from agricultural or natural landscapes with higher NDVI, NDWI, and SAVI values to urban development characterized by elevated LST, Brightness, and NDBI.

Figure 5 illustrates scatterplot relationships between PC1 of LST and all surface biophysical parameters, quantifying association strength and providing coefficient of determination values. The analysis reveals brightness, NDBI, and NDVI exhibit positive correlations with PC1 of LST, while SAVI, NDWI, Greenness, and Wetness demonstrate negative correlations, consistent with expected thermal influences.

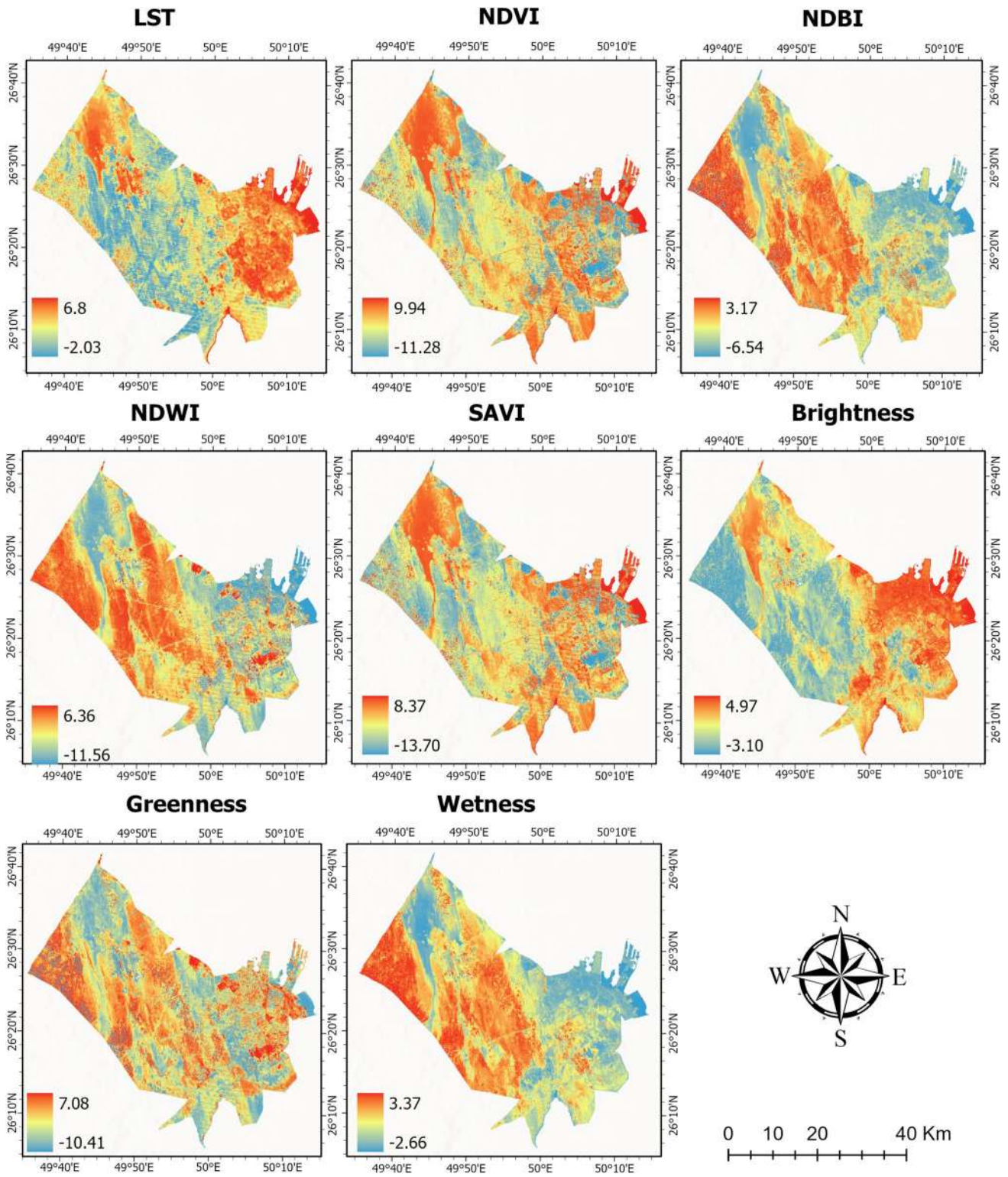

Fig. 4 PC1 figures of LST and other surface BPs

Among impervious surface parameters, Brightness accounts for 29% of LST variation while NDBI explains 28%, indicating surface brightness serves as a slightly more significant predictor than built-up density alone. For vegetation-related parameters, SAVI shows strongest association explaining 32% of variance, followed by NDVI at

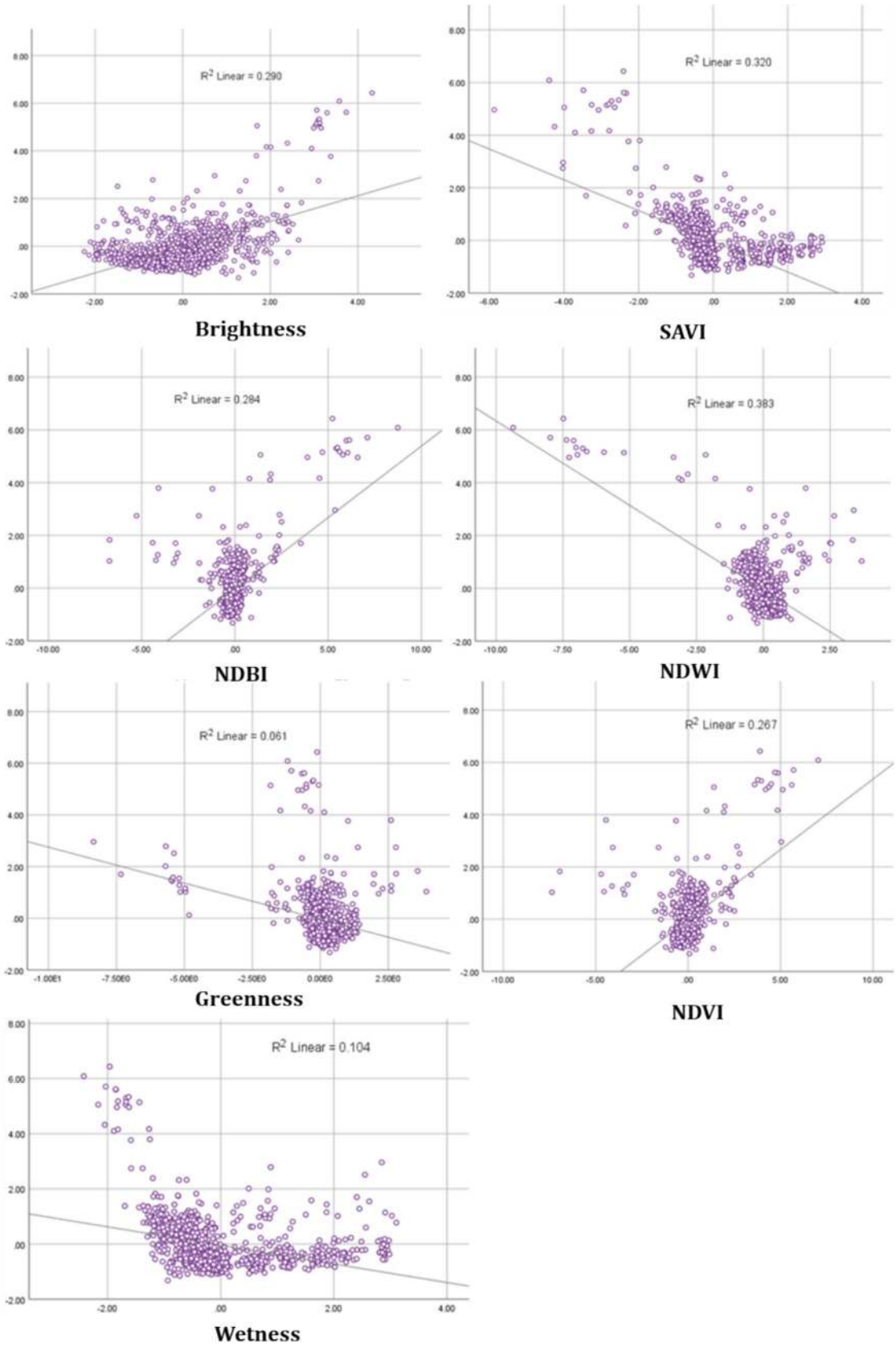

Fig. 5 Scatterplot between the PC1 of the LST and all surface BP

27%, while Greenness accounts for only 6%. Water-related parameters demonstrate the most significant relationships with LST. NDWI accounts for over 38% of LST variation, establishing it as the most influential single predictor, while Tasseled Cap Wetness explains only 10%, highlighting NDWI's superior performance in capturing moisture-related thermal effects in arid urban environments.

Biophysical parameter performance in LST prediction

Figure 6 presents standardized residuals between actual and predicted LST variations based on each surface biophysical parameter, providing comprehensive visual assessment of model performance. The residual maps illustrate spatial distribution of prediction discrepancies, with smaller residual magnitudes indicating superior model performance.

The residual analysis reveals distinct performance patterns among parameter categories. Water-related indices, particularly NDWI, demonstrate most consistent performance with relatively low residual values, confirming superior predictive capability in arid environments. NDWI residual maps show minimal prediction errors in areas with water features and higher soil moisture, while larger residuals appear in transitional zones were mixed land cover types of complicate moisture assessment.

Vegetation-related parameters exhibit variable residual patterns reflecting different sensitivities to arid conditions. NDVI residuals show moderate magnitudes with spatial clustering in sparse vegetation areas, while SAVI demonstrates more uniform residual distribution, confirming superior performance in soil-background affected environments. Greenness displays larger and more spatially variable residuals, indicating inconsistent predictive performance across different urban landscape types.

Built-up area indicators present contrasting residual characteristics. Brightness exhibits relatively small and uniformly distributed residuals, particularly in highly urbanized areas, confirming effectiveness as thermal predictor. NDBI shows larger residual magnitudes with more pronounced spatial clustering, suggesting less reliable prediction performance in certain urban contexts.

Table 3 presents comprehensive performance metrics for each biophysical parameter in predicting LST variations.

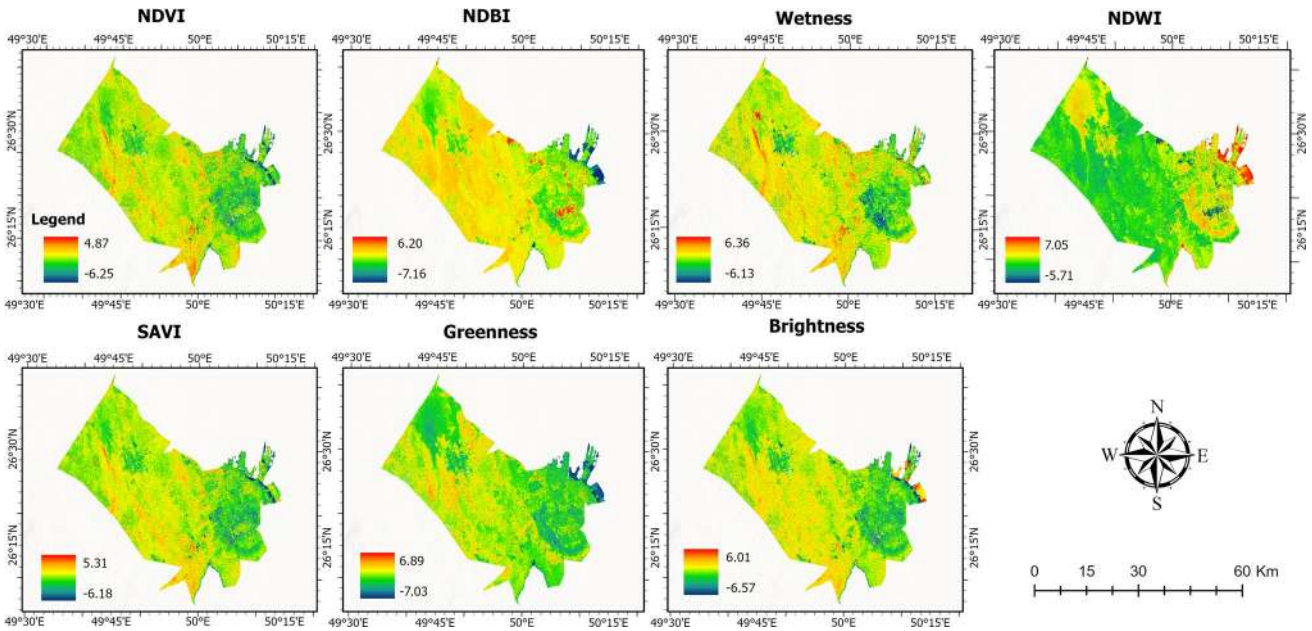

Fig. 6 Standard residual depending on each BP between the actual and expected fluctuations in LST

Table 3 Performance metrics of surface biophysical parameters for LST variations

Surface Biophysical Parameters	Brightness	Greenness	NDBI	NDVI	NDWI	SAVI	Wetness
Mean value of R	0.731	0.251	0.035	0.745	0.388	0.769	0.764
Standard deviation of R	0.397	0.564	0.258	0.388	0.537	0.372	0.376
Mean value of RMSE	0.495	0.842	0.832	0.492	0.785	0.455	0.450
Standard deviation of RMSE	0.471	0.648	0.807	0.4406	0.590	0.428	0.445

Among impervious surface indicators, Brightness emerges as superior predictor ($R^2 = 0.731$, RMSE = 0.495) compared to NDBI's weaker performance ($R^2 = 0.035$, RMSE = 0.832). Vegetation parameters show variable performance, with SAVI demonstrating strongest predictive capability ($R^2 = 0.769$, RMSE = 0.455), followed by NDVI ($R^2 = 0.745$, RMSE = 0.492). Water-related parameters demonstrate contrasting results, with Wetness showing stronger predictive performance ($R^2 = 0.764$, RMSE = 0.450) compared to NDWI ($R^2 = 0.388$, RMSE = 0.785), suggesting that Tasseled Cap Wetness component may capture broader moisture-related thermal effects than the band ratio approach.

ML Model performance and comparison

Figure 7 presents spatial distribution of modeled LST variations using Decision Tree (DT) and RF approaches, revealing systematic differences in prediction patterns. The RF model consistently displays higher temperature values (red colors) indicating elevated temperature regions, while the DT model predominantly shows lower temperature estimates (blue and yellow colors). This systematic difference reflects the RF model's superior capability in capturing complex urban thermal patterns through its ensemble learning approach.

Table 4 provides quantitative evaluation metrics comparing DT and RF model performance across multiple statistical measures. The RF model demonstrates superior performance across all evaluated parameters, with substantially lower Mean Squared Error (0.151 vs. 0.274) and higher explanatory power ($R^2 = 0.884$ vs. 0.761). The statistical significance levels ($p < 0.001$ for RF vs. $p = 0.03$ for DT) and reduced standard error (0.007 vs. 0.036) further confirm the RF model's superior reliability and precision. Additional validation metrics confirm model reliability: RF model achieved MAE of 1.67°C, RMSE of 2.14°C, and Mean Bias Error (MBE) of −0.23°C with cross-validation standard errors below 0.31°C across all folds. The DT model showed higher error variability with MAE of 2.41°C, RMSE of 2.89°C, and MBE of 0.67°C. Cross-validation results reveal the RF model's superior generalization capability with mean $R^2 = 0.884 \pm 0.025$ across five folds (range: 0.859–0.909) and mean RMSE = 1.96 ± 0.31°C. The DT model showed higher variability with mean $R^2 = 0.761 \pm 0.042$ (range: 0.719–0.803) and mean RMSE = 2.48 ± 0.28°C. The lower standard deviation in RF performance metrics confirms its superior consistency and reduced overfitting compared to the DT approach.

Table 4 Model evaluation of the predicted LST for both DT and RF model

Parameter	DT model	RF model
MSE	0.274	0.151
R^2	0.761	0.884
P	0.03	0.000
Standard Error	0.036	0.007

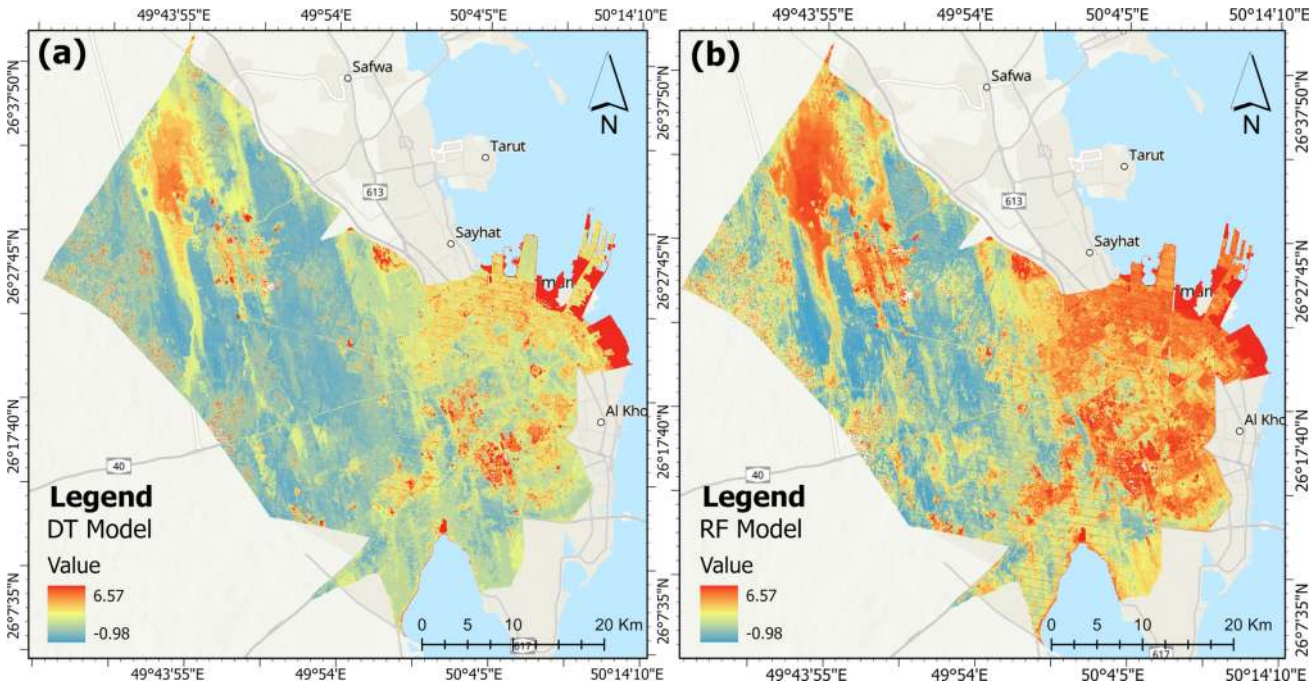

Fig. 7 Modeled LST variations by (**a**) DT model & (**b**) RF model

Figure 8 illustrates standardized residual patterns for both models, providing insights into prediction accuracy spatial distribution. The RF model produces residuals ranging from 5.25 to −3.96, while the DT model generates larger residuals from 6.72 to −5.23, confirming the RF model's superior prediction accuracy. The more constrained residual range for the RF model indicates more consistent performance across different urban landscape types.

Variable importance and uncertainty analysis

Figure 9 presents variable importance analysis for the RF model, revealing relative contribution of different biophysical parameters to LST prediction accuracy. NDWI emerges as the most influential variable, contributing 22.95% to model accuracy, emphasizing the paramount importance of water content and surface moisture in determining thermal patterns in arid environments. NDBI and NDVI follow as significant predictors, contributing 19.06% and 16.12% respectively, reflecting substantial influence of urbanization and vegetation coverage on thermal dynamics. Secondary variables including Wetness (15.158%), SAVI (12.704%), Brightness (8.2%), and Greenness (5.804%) provide complementary information for comprehensive thermal prediction. The combined contribution of water-related indices (NDWI and Wetness: 38.108%) substantially exceeds vegetation-related parameters (NDVI, SAVI, Greenness: 34.616%), highlighting

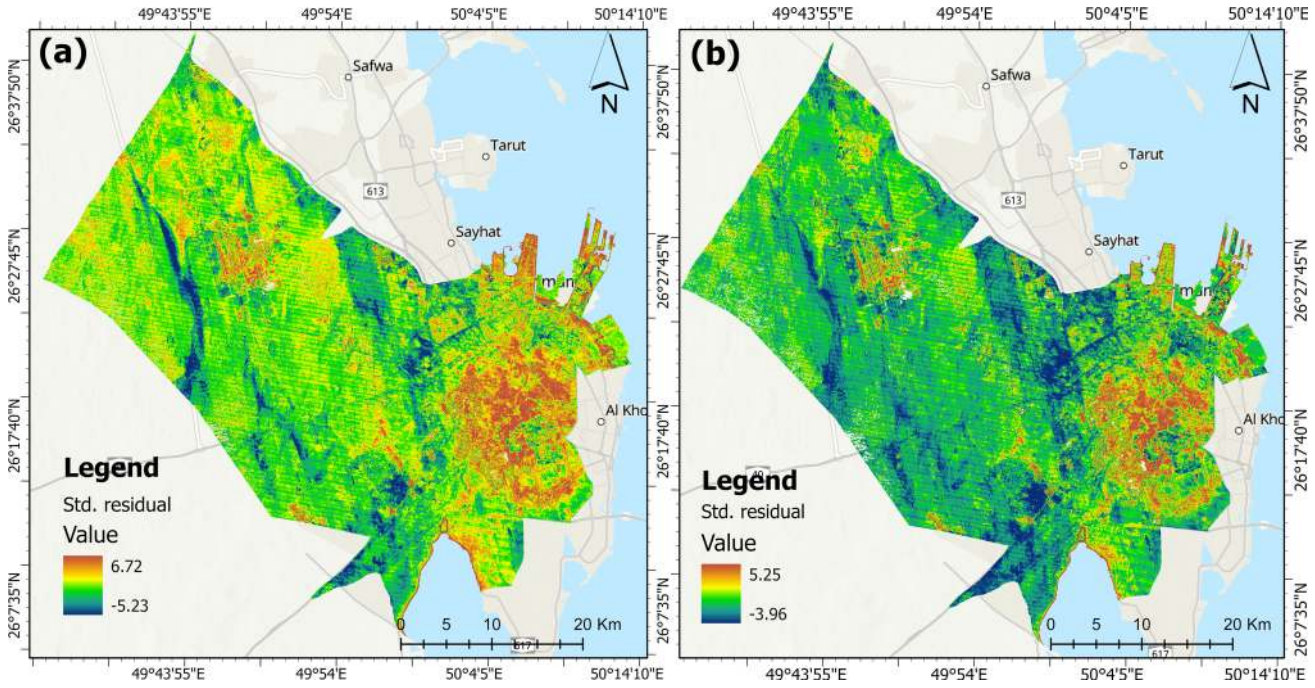

Fig. 8 Standard residual between the actual and predicted LST variations by (**a**) DT model & (**b**) RF model

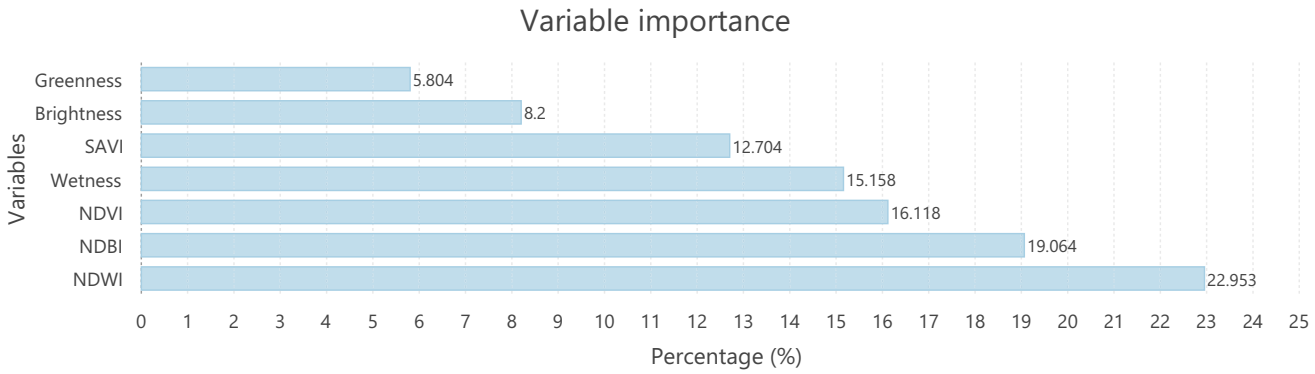

Fig. 9 Importance of the variables for predicting LST variations in the RF model

the critical role of moisture availability in LST regulation within arid urban environments.

Figures 10 and 11 present uncertainty analysis results, showing upper and lower bounds of the 90% prediction interval for the RF model across the urban landscape. The uncertainty analysis reveals spatial variation in prediction reliability, with prediction intervals ranging from ± 2.1°C in homogeneous vegetated areas to ± 3.4°C in highly heterogeneous urban-edge zones where mixed-pixel effects are more pronounced.

The uncertainty patterns reflect complexity of different urban landscape types, with higher uncertainty typically observed in transitional zones between different land cover classes. This spatial variation in prediction reliability is consistent with moderate-resolution satellite imagery limitations in complex urban environments and provides valuable guidance for interpreting model results across different urban contexts. Bootstrap resampling results ($n = 1000$) demonstrate that model performance is generally uniform across the study area, with slightly elevated prediction errors in areas undergoing rapid land use change. The comprehensive

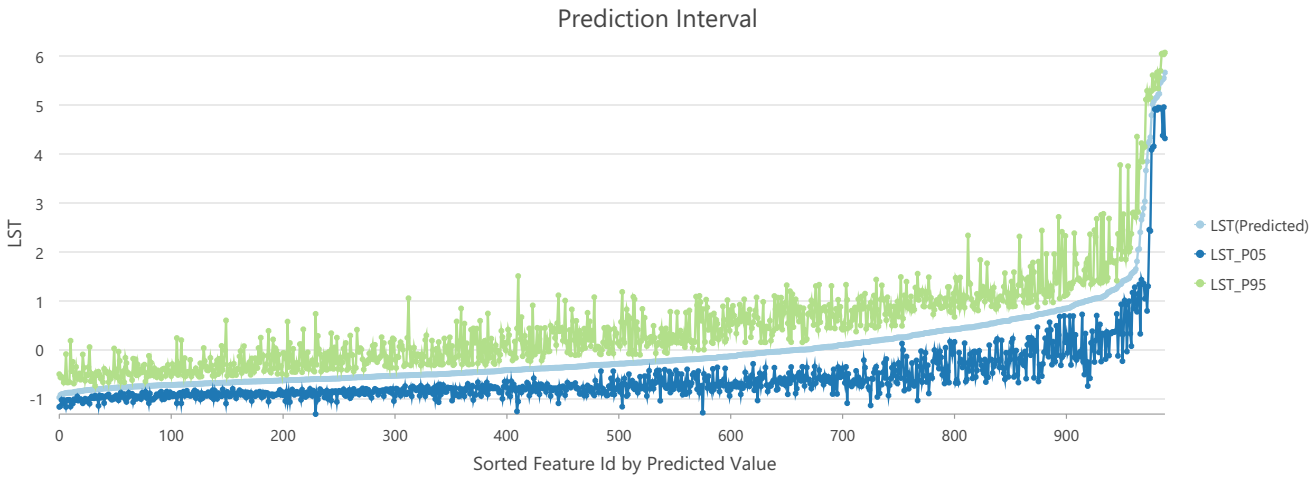

Fig. 10 Upper and lower bounds of the prediction interval with 90 percent confidence in the RF model

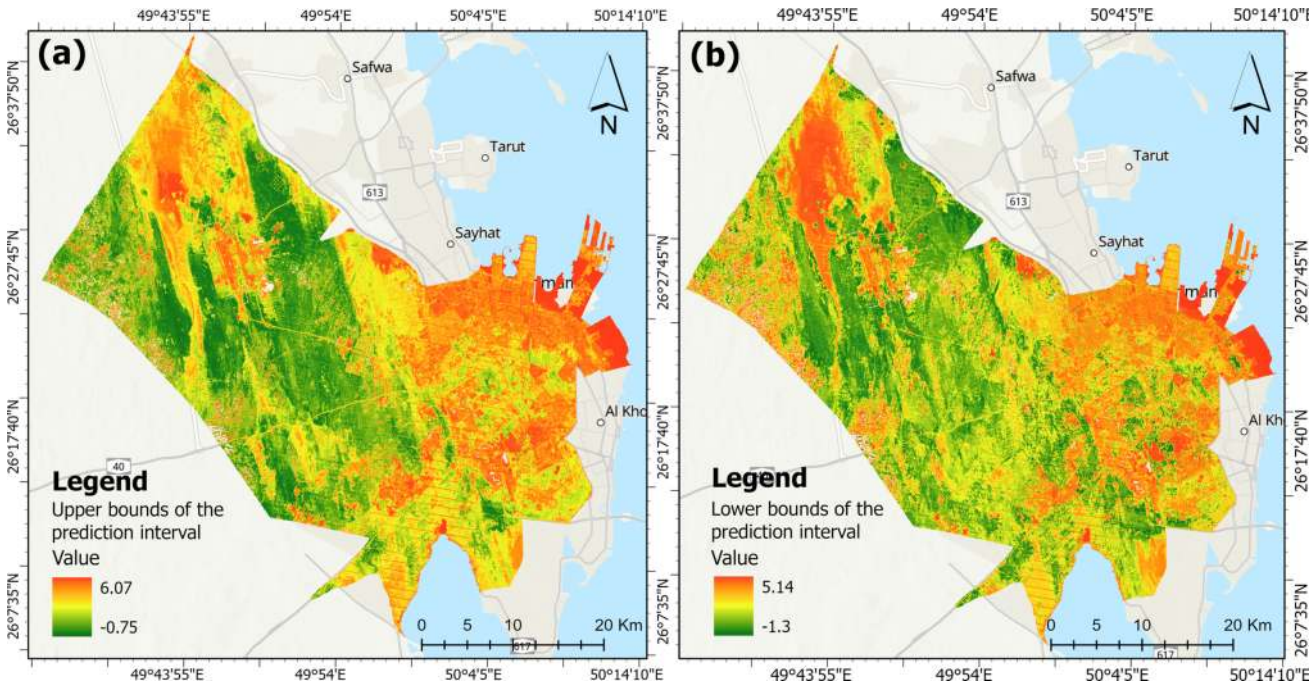

Fig. 11 Uncertainty parameter (**a**) Upper bound of the prediction interval (**b**) Lower bound of the prediction interval

uncertainty framework provides crucial information about prediction reliability and helps identify regions where additional calibration or alternative modeling approaches may be beneficial for improved thermal management applications.

Discussion

Temporal evolution of urban thermal environment

This research provides comprehensive evidence of dramatic thermal intensification over the past three decades, revealing alarming trends that reflect the intersection of rapid urbanization and extreme arid climate conditions. The systematic increase in mean LST from 29–32°C in 1993 to 44–47°C in 2023 represents a warming rate of 0.485°C/year ($p < 0.001$), substantially exceeding global urban warming trends reported in temperate regions. This accelerated thermal evolution aligns with broader patterns documented across the Arabian Gulf region, where similar cities have experienced comparable UHI intensification due to rapid development and extreme climatic conditions (Ahmed et al. 2024; Ashwini et al. 2024).

The exponential expansion of high-LST zones (> 44 °C) from 15% to 42% of the urban area represents a nearly threefold increase in extreme thermal stress zones, with built-up regions experiencing the most severe temperature increases at 0.627°C/year. This pattern is consistent with findings from neighboring arid cities, where rapid urbanization has created similar thermal stress conditions (Abdullah et al. 2022; Abulibdeh 2021). The accelerated warming post-2009, culminating in widespread areas exceeding 50°C by 2023, represents a critical threshold for human habitability and urban sustainability. These extreme temperatures approach the physiological limits for human thermal comfort and pose significant challenges for energy consumption, public health, and economic activities (Choudhury et al. 2019).

Biophysical parameter-LST relationships in arid environments

The correlation analysis reveals complex relationships between biophysical parameters and LST that demonstrate both consistencies and notable deviations from patterns reported in temperate urban environments. The exceptionally strong negative correlation between NDWI and LST ($r = -0.652$, 95% CI: −0.689 to −0.612) surpasses relationships typically observed in humid regions, highlighting the amplified importance of water features and surface moisture in arid urban thermal regulation (Guha et al. 2020a, b). This finding aligns with recent research in similar arid environments, where water bodies demonstrate disproportionately strong cooling effects compared to temperate cities (Ramaiah et al. 2020).

The moderate negative correlation between vegetation indices and LST (NDVI: $r = -0.259$; SAVI: $r = -0.363$) suggests that vegetation in arid environments has more limited cooling effectiveness compared to temperate cities, where stronger negative correlations are typically observed (Estoque et al. 2017; Guha & Govil 2022). This reduced cooling effectiveness may result from several factors specific to arid conditions, including low vegetation density, high evapotranspiration demand, and limited water availability that constrains plant physiological cooling processes (Feldman et al. 2023; Li et al. 2024).

The superior performance of SAVI over NDVI in correlation analysis reflects the challenges of vegetation assessment in arid environments where soil background interference significantly affects spectral signatures. The stronger correlation observed with SAVI ($r = -0.363$) compared to NDVI ($r = -0.259$) confirms the importance of soil background correction in water-limited environments where vegetation coverage is typically sparse and surrounded by bright soil or pavement surfaces (Sun et al. 2012).

The strong positive correlation between NDBI and LST ($r = 0.590$, 95% CI: 0.548 to 0.628) confirms the substantial thermal impact of built-up areas, consistent with findings from other rapidly urbanizing Middle Eastern cities (Chen et al. 2013; Guha et al. 2021). This relationship reflects the dominance of heat-absorbing materials such as asphalt, concrete, and glass that trap and re-radiate solar energy more effectively than natural surfaces.

Machine learning model performance and predictive capability

The superior performance of the RF model compared to Decision Tree approaches demonstrates the importance of ensemble learning methods for capturing complex thermal relationships in heterogeneous urban environments. The RF model's ability to explain 88% of LST variance ($R^2 = 0.884$) with substantially lower prediction error (MSE = 0.151 vs. 0.274) reflects its enhanced capacity to model non-linear relationships and interactions between multiple biophysical parameters (Rodriguez-Galiano et al. 2012).

The consistent performance of the RF model across five-fold cross-validation (mean $R^2 = 0.884 \pm 0.025$) demonstrates superior generalization capability compared to the Decision Tree approach (mean $R^2 = 0.761 \pm 0.042$), indicating reduced overfitting and more reliable prediction across different urban contexts. This finding aligns with recent studies comparing ML approaches for LST prediction, where ensemble methods consistently outperform single-model approaches in complex urban environments (Zhao et al. 2019; Yang et al. 2017).

The variable importance analysis reveals the dominance of water-related indices in thermal prediction, with NDWI contributing 22.95% to model accuracy, substantially exceeding vegetation-related parameters. This finding contrasts with studies in temperate regions where vegetation indices often dominate thermal prediction models, highlighting the unique characteristics of arid urban thermal dynamics (Pełechata et al. 2023; Zhang et al. 2022).

The combined contribution of water-related indices (NDWI, Wetness: 37.49%) substantially exceeds vegetation-related parameters (NDVI, SAVI, Greenness: 34.616%), emphasizing the critical role of moisture availability in LST regulation within arid urban environments. This dominance of water-related factors in thermal prediction models provides strong evidence for prioritizing water features and moisture management in urban planning strategies for arid cities (Liao et al. 2024; Syafii 2021).

Implications for urban planning and heat mitigation strategies

The quantitative findings from this study provide evidence-based foundation for developing targeted heat mitigation strategies specifically designed for rapidly urbanizing arid environments. The strong negative correlation between NDWI and LST ($r = -0.652$) supports recommendations for implementing water features at 300-500m intervals in areas where NDBI > 0.3 and LST > 45°C. Previous research suggests that strategic placement of water bodies could reduce local temperatures by 3–5°C based on observed relationships in similar arid urban contexts (Chen et al. 2013; Zhou et al. 2023).

The moderate but significant cooling effect of vegetation, despite arid constraints, supports mandatory minimum green space coverage requirements in high-temperature zones. Areas experiencing LST exceeding 44 °C should implement minimum 20% green space coverage in new developments, with careful selection of drought-resistant species that maximize cooling benefits while minimizing water consumption (Yao et al. 2020). The superior performance of SAVI over NDVI in correlation analysis suggests that vegetation management strategies should focus on soil moisture retention and species selection that minimize background interference effects.

Commercial and industrial zones exhibiting high brightness values (> 0.6) should implement cool roof policies and high-albedo pavement materials to reduce heat absorption. The positive correlation between brightness and LST ($r = 0.550$) indicates potential temperature reductions of 2–4°C through material modifications, representing a cost-effective intervention for existing urban areas (Wang et al. 2023; Yuan et al. 2021).

The identification of high-NDBI areas (> 0.4) experiencing LST > 46°C as "thermal stress zones" provides a framework for prioritizing interventions and restricting development density in the most vulnerable areas. These zones, representing 18% of the urban area as of 2023, require immediate attention to prevent further temperature escalation and protect public health (Abulibdeh 2021).

Methodological innovations and broader implications

The integrated methodological framework combining 30-year temporal analysis, Principal Component Analysis, and ensemble ML approaches provides a robust template for thermal analysis in similar arid urban environments. The systematic approach to cross-sensor calibration across Landsat missions ensures temporal consistency while maintaining high spatial resolution necessary for urban-scale analysis (Chander et al. 2009; Mishra et al. 2014).

The comprehensive uncertainty analysis using bootstrap resampling ($n = 1000$) with 90% prediction intervals provides crucial information for decision-making applications. The spatial variation in prediction uncertainty, ranging from ± 2.1°C in vegetated areas to ± 3.4°C in heterogeneous zones, acknowledges the inherent challenges of thermal prediction in complex urban environments while providing confidence bounds necessary for planning applications (Meinshausen 2006).

The research contributes valuable knowledge to urban climate science while offering actionable guidance for policymakers designing sustainable development initiatives that enhance environmental resilience under extreme climatic conditions. The findings support policy frameworks that integrate thermal considerations into urban planning processes, ensuring that future development contributes to rather than undermines urban resilience in extreme climatic conditions (Salim et al. 2024). The successful application of ML approaches for thermal prediction demonstrates the potential for evidence-based urban planning using readily available satellite data and computational resources, supporting sustainable development goals in challenging climatic conditions (Firozjaei et al. 2019).

Several limitations must be acknowledged. The 30 m Landsat resolution may underestimate micro-scale thermal variations in dense urban areas, while 16-day revisit cycles limit capture of rapid thermal changes (Mathew et al. 2024; Bisquert et al. 2016). The ML models, though accurate ($R^2 = 0.884$), are trained on historical data and may have reduced predictive power under novel climate conditions beyond the training envelope (Shafizadeh-Moghadam et al. 2020). Future research should integrate higher-resolution thermal imagery with LiDAR-derived urban morphology data and real-time IoT sensors to improve model accuracy

and temporal resolution (Kafy et al. 2024; Li et al. 2021). Additionally, incorporating socio-economic variables and deep learning techniques could enhance prediction capabilities and identify heat-vulnerable populations for targeted adaptation strategies.

Conclusion

This research effectively utilized a comprehensive analytical framework combining spatial analysis techniques, Principal Component Analysis, and advanced ML methods to elucidate LST dynamics and their relationship with biophysical parameters in Dammam City. The findings demonstrate the superior performance of the RF model over Decision Tree approaches in predicting LST variations, explaining 88% of thermal variance with substantially lower prediction errors (MSE = 0.151 vs. 0.274). The integration of 30-year temporal analysis with ensemble ML provides a robust methodological framework for understanding urban thermal environments in rapidly changing arid landscapes. Our analysis reveals alarming thermal intensification patterns across Dammam, with mean LST increasing from 29–32°C in 1993 to 44–47°C in 2023, representing a warming rate of 0.485°C/year that substantially exceeds global urban averages. The exponential expansion of extreme temperature zones (> 44 °C) from 15 to 42% of the urban area demonstrates the urgent scale of thermal stress affecting this rapidly developing arid city. Built-up regions experienced the most severe temperature increases at 0.627°C/year, confirming that urbanization intensity directly drives UHI amplification in water-limited environments. The statistical analysis reveals distinctive relationships between biophysical parameters and LST that differ markedly from patterns reported in temperate climates. Water-related indices demonstrated the strongest cooling potential, with NDWI exhibiting exceptional negative correlation ($r = -0.652$) and contributing 22.95% to model accuracy, followed by NDBI (19.06%) and NDVI (16.12%). The dominance of water-related parameters in thermal prediction models, accounting for 37.49% of combined explanatory power, highlights moisture availability as the critical factor in LST regulation within arid urban environments, exceeding the influence typically attributed to vegetation in temperate regions. Vegetation indices showed more limited cooling effectiveness (NDVI: $r = -0.259$; SAVI: $r = -0.363$) compared to temperate cities, reflecting the constraints of water scarcity, high evapotranspiration demand, and sparse vegetation coverage characteristic of arid environments. However, the superior performance of SAVI over NDVI confirms the importance of soil background correction in environments where vegetation assessment is complicated by bright surface interference. Conversely, urbanization indices exhibited strong positive correlations with LST, with NDBI ($r = 0.590$) and Brightness ($r = 0.550$) confirming the substantial thermal impact of impervious surfaces and urban materials. The comprehensive uncertainty analysis using bootstrap resampling ($n = 1000$) established 90% prediction intervals ranging from ± 2.1°C in vegetated areas to ± 3.4°C in heterogeneous zones, providing crucial confidence bounds for decision-making applications. This uncertainty quantification acknowledges inherent limitations while demonstrating the model's reliability for urban thermal management planning. These findings emphasize the urgent need for climate-sensitive urban planning strategies specifically designed for arid environments. Evidence-based recommendations include implementing water features at 300-500m intervals in high-NDBI zones (> 0.3), establishing mandatory 20% green space coverage in areas exceeding 44 °C, and designating thermal stress zones requiring restricted development density and enhanced cooling infrastructure. The research provides quantitative evidence that strategic integration of water features may offer more effective thermal mitigation than vegetation-focused approaches in water-limited environments.

This study establishes a robust methodological framework applicable to similar arid regions globally, supporting evidence-based urban planning through readily available satellite data and computational resources. The integration of temporal analysis, ML, and uncertainty quantification provides developing cities with practical tools for thermal monitoring and intervention planning. The research contributes valuable knowledge to urban climate science while offering actionable guidance for policymakers designing sustainable development initiatives that enhance environmental resilience under extreme climatic conditions. Future applications of this framework can support systematic thermal management in rapidly urbanizing arid regions, promoting sustainable development practices that prioritize human thermal comfort and urban habitability while acknowledging the unique constraints and opportunities present in water-limited environments.

Acknowledgements The authors extend their appreciation to the Ongoing Research Funding program (ORF-2025-848), King Saud University, Riyadh, Saudi Arabia.

Authors contributions Hamad Ahmed Altuwaijri: Project administration, Data collection, Funding acquisition, Formal analysis, Data curation, Supervision, Resources, Software, Methodology, Investigation, Writing – original draft, Validation, Writing – review & editing. Abdulla Al Kafy: Conceptualization, Project administration, Data collection, Formal analysis, Data curation, Supervision, Resources, Software, Methodology, Investigation, Writing – original draft, Validation, Writing – review & editing. Zullyadini A. Rahaman: Project administration, Resources, Supervision, Validation, Writing—review & editing. Jannatun Nahar Fariha: Data collection, Formal analysis, Data curation, Resources, Software, Methodology, Investigation, Writing – original draft, Writing – review & editing. Md Tanvir Miah: Data

collection, Formal analysis, Data curation, Supervision, Resources, Software, Methodology, Investigation, Writing – original draft, Writing – review & editing. Hrithik Nath: Methodology, Project administration, Resources, Supervision, Validation, Writing—review & editing. M Shahriar Sonet: Data curation, Project administration, Resources, Supervision, Validation, Writing—review & editing.

Funding This research work was supported by the Ongoing Research Funding program (ORF-2025-848), King Saud University, Riyadh, Saudi Arabia.

Data availability No datasets were generated or analysed during the current study.

Declarations

Ethics approval Not applicable.

Consent to participate Not applicable.

Consent for publication Not applicable.

Competing interests The authors declare no competing interests.

References

Abdullah S, Barua D, Abdullah Sk, Md A, Rabby YW (2022) Investigating the impact of land use/land cover change on present and future land surface temperature (LST) of chittagong. Bangladesh Earth Syst Environ 6(1):221–235. https://doi.org/10.1007/s41748-021-00291-w

Abulibdeh A (2021) Analysis of urban heat island characteristics and mitigation strategies for eight arid and semi-arid gulf region cities. Environ Earth Scie 80(7):259. https://doi.org/10.1007/s12665-021-09540-7

Addas A (2023) Understanding the relationship between urban biophysical composition and land surface temperature in a hot desert megacity (Saudi Arabia). Int J Environ Res Public Health 20(6):5025. https://doi.org/10.3390/ijerph20065025

Ahmed M, Aloshan MA, Mohammed W, Mesbah E, Alsaleh NA, Elghonaimy I (2024) Characterizing land surface temperature (LST) through remote sensing data for small-scale urban development projects in the gulf cooperation council (GCC). Sustainability 16(9):3873. https://doi.org/10.3390/su16093873

AlDousari AE, Kafy AA, Saha M, Fattah MA, Almulhim AI, Faisal AA, Al Rakib A, Jahir DMA, Rahaman ZA, Bakshi A, Shahrier M, Rahman MM (2022) Modelling the impacts of land use/land cover changing pattern on urban thermal characteristics in Kuwait. Sustain Cities Soc 86:104107. https://doi.org/10.1016/j.scs.2022.104107

AlDousari AE, Al Kafy A, Rahaman ZA (2025) Unveiling the dynamic interplay of biophysical, morphological, and temperature extremes in arid regions of Kuwait: decoding sustainable urban resilience by utilizing remote sensing techniques. Arab J Geosci 18:131. https://doi.org/10.1007/s12517-025-12266-6

Al-Shaibah B, Liu X, Zhang J, Tong Z, Zhang M, El-Zeiny A, Faichia C, Hussain M, Tayyab M (2021) Modeling water quality parameters using Landsat multispectral images: a case study of erlong lake. Northeast China Remote Sens 13(9):1603. https://doi.org/10.3390/rs13091603

Altuwaijri HA, Al Kafy A, Rahaman ZA (2025) Multi-temporal remote sensing and geospatial analysis for urban ecosystem service dynamics: a three-decade assessment of land surface transformation in Jeddah, Saudi Arabia. Phys Chem Earth, Parts a/b/c 139:103892. https://doi.org/10.1016/j.pce.2025.10389

Ashwini K, Sil BS, Kafy AA, Altuwaijri HA, Nath H, Rahaman ZA (2024) Harnessing machine learning algorithms to model the association between land use/land cover change and heatwave dynamics for enhanced environmental management. Land 13(8):1273. https://doi.org/10.3390/land13081273

Barsi J, Schott J, Hook S, Raqueno N, Markham B, Radocinski R (2014) Landsat-8 thermal infrared sensor (TIRS) vicarious radiometric calibration. Remote Sens 6(11):11607–11626. https://doi.org/10.3390/rs61111607

Bellón B, Bégué A, Lo Seen D, de Almeida C, Simões M (2017) A remote sensing approach for regional-scale mapping of agricultural land-use systems based on NDVI time series. Remote Sens 9(6):600. https://doi.org/10.3390/rs9060600

Bisquert M, Sanchez JM, Caselles V (2016) Evaluation of disaggregation methods for downscaling MODIS land surface temperature to landsat spatial resolution in barrax test site. IEEE J Sel Topics Appl Earth Obs Remote Sens 9(4):1430–1438. https://doi.org/10.1109/JSTARS.2016.2519099

Breiman L, Friedman JH, Olshen RA, Stone CJ (2017) Classification and regression trees. Routledge. https://doi.org/10.1201/9781315139470

Chander G, Markham BL, Helder DL (2009) Summary of current radiometric calibration coefficients for Landsat MSS, TM, ETM+, and EO-1 ALI sensors. Remote Sens Environ 113(5):893–903. https://doi.org/10.1016/j.rse.2009.01.007

Chen J, Zhu X, Vogelmann JE, Gao F, Jin S (2011) A simple and effective method for filling gaps in Landsat ETM+ SLC-off images. Remote Sens Environ 115(4):1053–1064. https://doi.org/10.1016/j.rse.2010.12.010

Chen L, Li M, Huang F, Xu S (2013) Relationships of LST to NDBI and NDVI in Wuhan City based on Landsat ETM+ image. 2013 6th International Congress on Image and Signal Processing (CISP). Hangzhou, China pp 840-845. https://doi.org/10.1109/CISP.2013.6745282

Choudhury D, Das K, Das A (2019) Assessment of land use land cover changes and its impact on variations of land surface temperature in asansol-durgapur development region. Egypt J Remote Sens Space Sci 22(2):203–218. https://doi.org/10.1016/j.ejrs.2018.05.004

Crank PJ, Middel A, Wagner M, Hoots D, Smith M, Brazel A (2020) Validation of seasonal mean radiant temperature simulations in hot arid urban climates. Sci Total Environ 749:141392. https://doi.org/10.1016/j.scitotenv.2020.141392

Dalal SG, Shirodkar PV, Jagtap TG, Naik BG, Rao GS (2010) Evaluation of significant sources influencing the variation of water quality of Kandla creek, Gulf of Katchchh, using PCA. Environ Monit Assess 163(1–4):49–56. https://doi.org/10.1007/s10661-009-0815-y

Das DN, Chakraborti S, Saha G, Banerjee A, Singh D (2020) Analysing the dynamic relationship of land surface temperature and landuse pattern: a city level analysis of two climatic regions in India. City Environ Interact 8:100046. https://doi.org/10.1016/j.cacint.2020.100046

Das M, Das A, Ghosh S, Sarkar R, Saha S (2021) Spatio-temporal concentration of atmospheric particulate matter (PM2.5) during pandemic: a study on most polluted cities of indo-gangetic plain. Urban Climate 35:100758. https://doi.org/10.1016/j.uclim.2020.100758

El Fellah S, Rziza M, El Haziti M (2017) An efficient approach for filling gaps in landsat 7 satellite images. IEEE Geosci Remote Sens Lett 14(1):62–66. https://doi.org/10.1109/LGRS.2016.2626138

Estoque RC, Murayama Y, Myint SW (2017) Effects of landscape composition and pattern on land surface temperature: an urban heat island study in the megacities of Southeast Asia. Sci Total Environ 577:349–359. https://doi.org/10.1016/j.scitotenv.2016.10.195

Faisal AA, Kafy AA, Al Rakib A, Akter KS, Jahir DMA, Sikdar MS, Ashrafi TJ, Mallik S, Rahman MM (2021) Assessing and predicting land use/land cover, land surface temperature and urban thermal field variance index using Landsat imagery for Dhaka Metropolitan area. Environ Challenges 4:100192. https://doi.org/10.1016/j.envc.2021.100192

Feldman AF, Short Gianotti DJ, Dong J, Trigo IF, Salvucci GD, Entekhabi D (2023) Tropical surface temperature response to vegetation cover changes and the role of drylands. Glob Change Biol 29(1):110–125. https://doi.org/10.1111/gcb.16455

Firozjaei A, Liu S, Mijani K, Weng Q (2019) A PCA–OLS model for assessing the impact of surface biophysical parameters on land surface temperature variations. Remote Sens 11(18):2094. https://doi.org/10.3390/rs11182094

Gaitani N, Burud I, Thiis T, Santamouris M (2017) High-resolution spectral mapping of urban thermal properties with unmanned aerial vehicles. Build Environ 121:215–224. https://doi.org/10.1016/j.buildenv.2017.05.027

Ghosh A, Joshi PK (2014) Hyperspectral imagery for disaggregation of land surface temperature with selected regression algorithms over different land use land cover scenes. ISPRS J Photogramm Remote Sens 96:76–93. https://doi.org/10.1016/j.isprsjprs.2014.07.003

Gogoi PP, Vinoj V, Swain D, Roberts G, Dash J, Tripathy S (2019) Land use and land cover change effect on surface temperature over Eastern India. Sci Rep 9(1):8859. https://doi.org/10.1038/s41598-019-45213-z

Gourfi A, Taïbi AN, Salhi S, Hannani ME, Boujrouf S (2022) The surface urban heat island and key mitigation factors in arid climate cities, case of Marrakesh. Morocco Remote Sens 14(16):3935. https://doi.org/10.3390/rs14163935

Guha S, Govil H (2022) Seasonal impact on the relationship between land surface temperature and normalized difference vegetation index in an urban landscape. Geocarto Int 37(8):2252–2272. https://doi.org/10.1080/10106049.2020.1815867

Guha S, Govil H, Besoya M (2020a) An investigation on seasonal variability between LST and NDWI in an urban environment using Landsat satellite data. Geomat Nat Haz Risk 11(1):1319–1345. https://doi.org/10.1080/19475705.2020.1789762

Guha S, Govil H, Diwan P (2020b) Monitoring LST-NDVI relationship using premonsoon landsat datasets. Advances in Meteorology 2020:1–15. https://doi.org/10.1155/2020/4539684

Guha S, Govil H, Gill N, Dey A (2021) A long-term seasonal analysis on the relationship between LST and NDBI using Landsat data. Quatern Int 575–576:249–258. https://doi.org/10.1016/j.quaint.2020.06.041

Hall-Beyer M (2003) Comparison of single-year and multiyear ndvi time series principal components in cold temperate biomes. IEEE Trans Geosci Remote Sens 41(11):2568–2574. https://doi.org/10.1109/TGRS.2003.817274

Han D, Zhang T, Qin Y, Tan Y, Liu J (2023) A comparative review on the mitigation strategies of urban heat island (UHI): a pathway for sustainable urban development. Climate Dev 15(5):379–403. https://doi.org/10.1080/17565529.2022.2092051

https://ladsweb.nascom.nasa.gov. (n.d.-b). *USGS*. United States Geological Survey. Available Online.

https://ladsweb.nascom.nasa.gov . (n.d.-a). LAADS DAAC. Level-1 and Atmosphere Archive and Distribution System Distributed Active Archive Center. Available online.

Hussain S, Mubeen M, Ahmad A, Majeed H, Qaisrani SA, Hammad HM, Amjad M, Ahmad I, Fahad S, Ahmad N, Nasim W (2023) Assessment of land use/land cover changes and its effect on land surface temperature using remote sensing techniques in Southern Punjab. Pak Environ Sci Pollut Res 30(44):99202–99218. https://doi.org/10.1007/s11356-022-21650-8

Hussain S, Lu L, Mubeen M, Nasim W, Karuppannan S, Fahad S, Tariq A, Mousa BG, Mumtaz F, Aslam M (2022) Spatiotemporal variation in land use land cover in the response to local climate change using multispectral remote sensing data. Land, 11(5). https://doi.org/10.3390/land11050595

Hutcheson G, Hutcheson G (2011) Ordinary least-squares regression. In The SAGE Dictionary of Quantitative Management Research (pp. 225–228). SAGE Publications Ltd. https://doi.org/10.4135/9781446251119.n67

Irulappa-Pillai-Vijayakumar D B, Renaud JP, Morneau F, McRoberts RE, Vega C (2019) Increasing precision for French forest inventory estimates using the k-NN technique with optical and photogrammetric data and model-assisted estimators. Remote Sens 11(8):991. https://doi.org/10.3390/rs11080991

Jimenez-Munoz JC, Sobrino JA, Skokovic D, Mattar C, Cristobal J (2014) Land surface temperature retrieval methods from landsat-8 thermal infrared sensor data. IEEE Geosci Remote Sens Lett 11(10):1840–1843. https://doi.org/10.1109/LGRS.2014.2312032

Jiménez-Muñoz JC, Sobrino JA (2003) A generalized single-channel method for retrieving land surface temperature from remote sensing data. J Geophys Res: Atmospheres, 108(D22). https://doi.org/10.1029/2003JD003480

Kafy AA, Crews KA, Thompson AE (2024) Exploring the cooling potential of green roofs for mitigating diurnal heat island intensity by utilizing Lidar and Artificial Neural Network. Sustain Cities Soc 116:105893. https://doi.org/10.1016/j.scs.2024.105893

Kafy AAl, Dey NN, Al Rakib A, Rahaman ZA, Nasher NMR, Bhatt A (2021) Modeling the relationship between land use/land cover and land surface temperature in Dhaka, Bangladesh using CA-ANN algorithm. Environ Challenges, 4. https://doi.org/10.1016/j.envc.2021.100190

Kumar BP, Babu KR, Anusha BN, Rajasekhar M (2022) Geo-environmental monitoring and assessment of land degradation and desertification in the semi-arid regions using Landsat 8 OLI / TIRS, LST, and NDVI approach. Environ Challenges 8:100578. https://doi.org/10.1016/j.envc.2022.100578

Li T, Jiang Z, Treut HL, Li L, Zhao L, Ge L (2021) Machine learning to optimize climate projection over China with multi-model ensemble simulations. Environ Res Lett 16(9):094028. https://doi.org/10.1088/1748-9326/ac1d0c

Li G, Fang C, Li Y, Wang Z, Sun S, He S, Qi W, Bao C, Ma H, Fan Y, Feng Y, Liu X (2022) Global impacts of future urban expansion on terrestrial vertebrate diversity. Nat Commun 13(1):1628. https://doi.org/10.1038/s41467-022-29324-2

Li Z, Bai X, Tan Q, Zhao C, Li Y, Luo G, Chen F, Li C, Ran C, Zhang S, Xiong L, Song F, Du C, Xiao B, Xue Y, Long M (2024) Dryness stress weakens the sustainability of global vegetation cooling. Sci Total Environ 909:168474. https://doi.org/10.1016/j.scitotenv.2023.168474

Liao M-C, Sung W-P, Chen Shi Q-Q (2024) Comparing small water bodies' impact on subtropical campus outdoor temperature: measured vs. simulated data. Buildings 14(5):1288. https://doi.org/10.3390/buildings14051288

Liu Y, Qian J, Yue H (2021a) Comparison and evaluation of different dryness indices based on vegetation indices-land surface temperature/albedo feature space. Adv Space Res 68(7):2791–2803. https://doi.org/10.1016/j.asr.2021.05.007

Liu Z, Ying H, Chen M, Bai J, Xue Y, Yin Y, Batchelor WD, Yang Y, Bai Z, Du M, Guo Y, Zhang Q, Cui Z, Zhang F, Dou Z (2021b) Optimization of China's maize and soy production can ensure feed sufficiency at lower nitrogen and carbon footprints. Nature Food 2(6):426–433. https://doi.org/10.1038/s43016-021-00300-1

Liu X, Al-Shaibah B, Zhao C, Tong Z, Bian H, Zhang F, Zhang J, Pei X (2022) Estimation of the key water quality parameters in the surface water, middle of northeast China, based on gaussian

process regression. Remote Sens 14(24):6323. https://doi.org/10.3390/rs14246323
Malbéteau Y, Merlin O, Gascoin S, Gastellu JP, Mattar C, Olivera-Guerra L, Khabba S, Jarlan L (2017) Normalizing land surface temperature data for elevation and illumination effects in mountainous areas: a case study using ASTER data over a steep-sided valley in Morocco. Remote Sens Environ 189:25–39. https://doi.org/10.1016/j.rse.2016.11.010
Mas J-F (1999) Monitoring land-cover changes: a comparison of change detection techniques. Int J Remote Sens 20(1):139–152. https://doi.org/10.1080/014311699213659
Mathew A, Arunab KS, Kumar Sharma A (2024) Revealing the urban heat Island: Investigating spatiotemporal surface temperature dynamics, modeling, and interactions with controllable and non-controllable factors. Remote Sens Appl: Soc Environ 35:101219. https://doi.org/10.1016/j.rsase.2024.101219
Meinshausen N (2006) Quantile regression forests. J Mach Learn Res 7:983–999
Mirzaee S, Mirzakhani Nafchi A (2023) Monitoring spatiotemporal vegetation response to drought using remote sensing data. Sensors 23(4):2134. https://doi.org/10.3390/s23042134
Mishra N, Haque M, Leigh L, Aaron D, Helder D, Markham B (2014) Radiometric cross calibration of landsat 8 operational land imager (OLI) and landsat 7 enhanced thematic mapper plus (ETM+). Remote Sens 6(12):12619–12638. https://doi.org/10.3390/rs61212619
Mukherjee F, Singh D (2020) Assessing land use-land cover change and its impact on land surface temperature using LANDSAT data: a comparison of two urban areas in India. Earth Syst Environ 4(2):385–407. https://doi.org/10.1007/s41748-020-00155-9
Pełechata A, Kufel L, Pukacz A, Strzałek M, Biardzka E, Brzozowski M, Kaczmarek L, Pełechaty M (2023) Climate features or the composition of submerged vegetation? Which factor has a greater impact on the phytoplankton structure in temperate lakes? Ecol Ind 146:109840. https://doi.org/10.1016/j.ecolind.2022.109840
Quinlan JR (1993) CHAPTER 5 - from trees to rules. In J. R. QUINLAN (Ed.), *C4.5* (pp. 45–56). Morgan Kaufmann. https://doi.org/10.1016/B978-0-08-050058-4.50010-3
Rad AM, Kreitler J, Sadegh M (2021) Augmented normalized difference water index for improved surface water monitoring . Environ Model Softw 140:105030. https://doi.org/10.1016/j.envsoft.2021.105030
Rahman MT, Aldosary AS, Mortoja MdG (2017) Modeling future land cover changes and their effects on the land surface temperatures in the Saudi Arabian eastern coastal City of Dammam. Land 6(2):36. https://doi.org/10.3390/land6020036
Ramaiah M, Avtar R, Rahman MdM (2020) Land cover influences on LST in two proposed smart Cities of India: comparative analysis using spectral indices. Land 9(9):292. https://doi.org/10.3390/land9090292
Ren H, Zhou G, Zhang F (2018) Using negative soil adjustment factor in soil-adjusted vegetation index (SAVI) for aboveground living biomass estimation in arid grasslands. Remote Sens Environ 209:439–445. https://doi.org/10.1016/j.rse.2018.02.068
Rodriguez-Galiano VF, Ghimire B, Rogan J, Chica-Olmo M, Rigol-Sanchez JP (2012) An assessment of the effectiveness of a random forest classifier for land-cover classification. ISPRS J Photogramm Remote Sens 67:93–104. https://doi.org/10.1016/j.isprsjprs.2011.11.002
Salim MZ, Choudhari N, Kafy A-A, Nath H, Alsulamy S, Rahaman ZA, Aldosary AS, Rahmand MT, Al-Ramadan B (2024) A comprehensive review of navigating urbanization induced climate change complexities for sustainable groundwater resources management in the Indian subcontinent. Groundw Sustain Dev 25:101115. https://doi.org/10.1016/j.gsd.2024.101115
Sattari F, Hashim M, Pour AB (2018) Thermal sharpening of land surface temperature maps based on the impervious surface index with the TsHARP method to ASTER satellite data: a case study from the metropolitan Kuala Lumpur, Malaysia. Measurement 125:262–278. https://doi.org/10.1016/j.measurement.2018.04.092
Shafizadeh-Moghadam H, Weng Q, Liu H, Valavi R (2020) Modeling the spatial variation of urban land surface temperature in relation to environmental and anthropogenic factors: a case study of Tehran. Iran Giscience Remote Sens 57(4):483–496. https://doi.org/10.1080/15481603.2020.1736857
Simkin RD, Seto KC, McDonald RI, Jetz W (2022). Biodiversity impacts and conservation implications of urban land expansion projected to 2050. Proc National Acad Sci, 119(12). https://doi.org/10.1073/pnas.2117297119
Sobrino JA, Jimenez-Munoz JC, Soria G, Romaguera M, Guanter L, Moreno J, Plaza A, Martinez P (2008) Land surface emissivity retrieval from different VNIR and TIR sensors. IEEE Trans Geosci Remote Sens 46(2):316–327. https://doi.org/10.1109/TGRS.2007.904834
Sonet MS, Hasan MY, Kafy A et al (2025) Spatiotemporal analysis of urban expansion, land use dynamics, and thermal characteristics in a rapidly growing megacity using remote sensing and machine learning techniques. Theor Appl Climatol 156:79. https://doi.org/10.1007/s00704-024-05264-3
Sun Q, Wu Z, Tan J (2012) The relationship between land surface temperature and land use/land cover in Guangzhou. China Environ Earth Sci 65(6):1687–1694. https://doi.org/10.1007/s12665-011-1145-2
Surasinghe TD, Singh KK, Smart LS (2025) Leveraging phenology to assess seasonal variations of plant communities for mapping dynamic ecosystems. Remote Sens 17(10):1778. https://doi.org/10.3390/rs17101778
Syafii N (2021) Promoting urban water bodies as a potential strategy to improve urban thermal environment. Geographica Pannonica 25(2):113–120. https://doi.org/10.5937/gp25-30431
Tabassum A, Hong SH, Park K et al (2024) Impacts of changes in soil moisture on urban heat islands and urban breeze circulations: idealized ensemble simulations. Asia-Pac J Atmos Sci 60:541–553. https://doi.org/10.1007/s13143-024-00369-1
Wang Z, Li X, Mao Y, Li L, Wang X, Lin Q (2022) Dynamic simulation of land use change and assessment of carbon storage based on climate change scenarios at the city level: a case study of Bortala. China Ecol Indic 134:108499. https://doi.org/10.1016/j.ecolind.2021.108499
Wang J, Meng F, Lu H, Lv Y, Jing T (2023) Individual and combined effects of 3D buildings and green spaces on the urban thermal environment: a case study in Jinan. China Atmosphere 14(6):908. https://doi.org/10.3390/atmos14060908
Weng Q, Lu D, Schubring J (2004) Estimation of land surface temperature–vegetation abundance relationship for urban heat island studies. Remote Sens Environ 89(4):467–483. https://doi.org/10.1016/j.rse.2003.11.005
Weng Q, Rajasekar U, Hu X (2011) Modeling urban heat islands and their relationship with impervious surface and vegetation abundance by using ASTER images. IEEE Trans Geosci Remote Sens 49(10):4080–4089. https://doi.org/10.1109/TGRS.2011.2128874
Weng Q, Firozjaei MK, Kiavarz M, Alavipanah SK, Hamzeh S (2019a) Normalizing land surface temperature for environmental parameters in mountainous and urban areas of a cold semi-arid climate. Sci Total Environ 650:515–529. https://doi.org/10.1016/j.scitotenv.2018.09.027
Weng Q, Firozjaei MK, Sedighi A, Kiavarz M, Alavipanah SK (2019b) Statistical analysis of surface urban heat island intensity variations: a case study of Babol city. Iran Giscience Remote Sens 56(4):576–604. https://doi.org/10.1080/15481603.2018.1548080

Wu Y, Li S, Yu S (2016) Monitoring urban expansion and its effects on land use and land cover changes in Guangzhou City. China Environ Monit Assess 188(1):54. https://doi.org/10.1007/s10661-015-5069-2

Xu M, Watanachaturaporn P, Varshney P, Manoj A (2005) Decision tree regression for soft classification of remote sensing data. Remote Sens Environ 97(3):322–336. https://doi.org/10.1016/j.rse.2005.05.008

Yang Y, Cao C, Pan X, Li X, Zhu X (2017) Downscaling land surface temperature in an arid area by using multiple remote sensing indices with random forest regression. Remote Sens 9(8):789. https://doi.org/10.3390/rs9080789

Yao L, Li T, Xu M, Xu Y (2020) How the landscape features of urban green space impact seasonal land surface temperatures at a city-block-scale: an urban heat island study in Beijing. China Urban Forestry Urban Green 52:126704. https://doi.org/10.1016/j.ufug.2020.126704

Yu X, Guo X, Wu Z (2014) Land surface temperature retrieval from landsat 8 TIRS—comparison between radiative transfer equation-based method, split window algorithm and single channel method. Remote Sens 6(10):9829–9852. https://doi.org/10.3390/rs6109829

Yuan B, Zhou L, Dang X, Sun D, Hu F, Mu H (2021) Separate and combined effects of 3D building features and urban green space on land surface temperature. J Environ Manage 295:113116. https://doi.org/10.1016/j.jenvman.2021.113116

Yuan J, Lin Q, Chen S, Zhao H, Xie X, Cai Z, Zhang J, Cheng T, Hua M, Zhang R (2022) Influence of global warming and urbanization on regional climate of megacity: a case study of Chengdu. China Urban Climate 44:101227. https://doi.org/10.1016/j.uclim.2022.101227

Zhang H, Zhan C, Xia J, Yeh PJ-F (2022) Responses of vegetation to changes in terrestrial water storage and temperature in global mountainous regions. Sci Total Environ 851:158416. https://doi.org/10.1016/j.scitotenv.2022.158416

Zhao W, Duan S-B, Li A, Yin G (2019) A practical method for reducing terrain effect on land surface temperature using random forest regression. Remote Sens Environ 221:635–649. https://doi.org/10.1016/j.rse.2018.12.008

Zhou W, Cao W, Wu T, Zhang T (2023) The win-win interaction between integrated blue and green space on urban cooling. Sci Total Environ 863:160712. https://doi.org/10.1016/j.scitotenv.2022.160712

Authors and Affiliations

Hamad Ahmed Altuwaijri[1] · Abdulla Al Kafy[2] · Zullyadini A. Rahaman[3] · Jannatun Nahar Fariha[4] · Md Tanvir Miah[4] · Remon Ahmed Mishu[4] · Hrithik Nath[5,6] · M Shahriar Sonet[7,8]

✉ Hamad Ahmed Altuwaijri
haaltuwaijri@ksu.edu.sa

✉ Abdulla Al Kafy
abdullaalkafy@utexas.edu;
abdulla-al.kafy@localpathways.org

Zullyadini A. Rahaman
zully@fsk.upsi.edu.my

Jannatun Nahar Fariha
farihajannat720@gmail.com

Md Tanvir Miah
tanvir180417@gmail.com

Remon Ahmed Mishu
remon.mishu@gmail.com

Hrithik Nath
hrithiknath.ce@gmail.com

M Shahriar Sonet
mshahriar.sonet@utdallas.edu

[1] Department of Geography, College of Humanities and Social Sciences, King Saud University, 11451 Riyadh, Saudi Arabia

[2] Department of Geography & the Environment, The University of Texas at Austin, 1 University Station A3100, Austin, TX 78712, USA

[3] Department of Geography & Environment, Faculty of Human Sciences, Sultan Idris Education University, 35900 Tanjung Malim, Malaysia

[4] Urban and Rural Planning Discipline, Khulna University, Khulna 9208, Bangladesh

[5] Department of Civil Engineering, Khulna University of Engineering & Technology (KUET), Khulna 9203, Bangladesh

[6] Department of Civil Engineering, University of Creative Technology Chittagong (UCTC), Chattogram 4212, Bangladesh

[7] Geospatial Information Sciences, The University of Texas at Dallas, Dallas, TX 75080, USA

[8] Department of Geosciences, Center for Geospatial Technology, Texas Tech University, Lubbock, TX 79409, USA